POLITECNICO
MILANO 1863

SCUOLA DI INGEGNERIA INDUSTRIALE
E DELL'INFORMAZIONE

# Enhanced mid-fidelity modeling of distributed propulsion for aircraft preliminary design

Tesi di Laurea Magistrale in
Aeronautical Engineering - Ingegneria Aeronautica

Author: **Gianluca Vighi**
Student ID: 953611

Advisor: Prof. Lorenzo Trainelli
Co-advisors: Yasir Mahmood Khan
Academic Year: 2022-2023

# Abstract

Reducing pollutant emissions is one of the main goals of technological progress, in fact, many studies for cleaner aviation have been carried out in recent years.
The main aim to achieve of this thesis is the integration of a meta-model equipped with distributed electric propulsion (DEP) and fitted with plain flaps, into a sizing routine for pure electric and hybrid electric aircraft (TITAN).
In this work, plain flaps are used, a type of flap that has the advantage of being simple both in terms of construction, modelling with OpenVSP and prediction of the aerodynamic model trend;
Furthermore, they are a valid choice for the type of aircraft studied.
It is verified that the trend of behaviour with flap deflection, obtained with VLM simulations, corresponds to the one hypothesised.
The use of this meta-model allows to take into account the aeropropulsive interaction between the propellers and the wing.
The refinement of the meta-model with flap allows a more precise determination of the aeropropulsive interaction for the take-off and landing flight configuration.

**Keywords:** vortex lattice method, distributed electric propulsion, preliminary aircraft sizing, meta-model, aero-propulsive interaction, plain flap.

# Sintesi

La riduzione delle emissioni inquinanti è uno dei principali obiettivi del progresso tecnologico, infatti, da un po' di anni sono in corso numerosi studi per rendere l'aviazione più ecologica.
Lo scopo principale di questa tesi è l'integrazione di un meta-modello, dotato di propulsione elettrica distribuita (DEP) e di plain flap, in una routine di dimensionamento per velivoli elettrici puri e ibridi elettrici (TITAN).
In questo lavoro vengono utilizzati i plain flap, siccome questi hanno il vantaggio di essere semplici sia in termini di costruzione, modellazione con OpenVSP e nella previsione dell'andamento dell'effetto aerodinamico;
Inoltre rappresentano una valida scelta per la tipologia di velivolo studiata.
E' stato quindi verificato che il comportamento al variare della deflessione dei flap, ottenuto con le simulazioni VLM, corrisponda a quello ipotizzato.
L'utilizzo di questo meta-modello permette di tenere conto dell'interazione aeropropulsiva tra le eliche e l'ala.
L'affinamento del metamodello con i flap permette una determinazione più precisa dell'interazione aeropropulsiva per la configurazione di volo di decollo e atterraggio.

**Parole chiave:** metodo vortex lattice, propulsione elettrica distribuita, dimensionamento preliminare di velivoli, meta-modello, interazione aero-propulsiva, flap semplici.

# Ringraziamenti

Con questo elaborato termina questo mio percorso, lungo e non banale da portare a termine fino alla fine. Ci tengo quindi a ringraziare innanzitutto il mio relatore, Professor Lorenzo Trainelli, che mi ha dato la possibilità di finire i miei studi lavorando a questo progetto. Grazie ancora al Professor Lorenzo Trainelli e a Yasir Khan per il supporto e la pazienza nei miei confronti avuta durante questa attività di tesi. Un immenso grazie va poi a tutta la mia famiglia, che mi ha supportato e sopportato rendendo possibile questo percorso. Grazie a tutti i miei amici, in primis Tommaso Brienza, ma davvero tutti voi, nessuno escluso; Perchè senza questi legami di amicizia non avremmo la forza di affrontare le difficoltà della vita. Anche se non ho fatto nomi per non dilungarmi troppo, ci tengo ancora una volta a regalarvi un sincero GRAZIE A TUTTI!!!

# Contents

# 1 | Introduction

Reducing pollutant emissions is one of the main goals of technological progress.
The same trend can be observed in aviation, with several publicly funded projects such as NASA's Advanced Air Transport Technology [3] or the European Clean Aviation Program [1] aimed at finding new solutions for more sustainable aviation.
At present, electric propulsion seems to be a possible and the best strategy to achieve this goal; However, given the current energy density of batteries and therefore their weight, technological advances in battery performance will be needed to achieve fully electric commercial vehicles.
However, there are also advantages to using electric propulsion; In fact, the scalability of electric motors can allow a greater number of motors to be installed along the wing, with important aerodynamic effects due to the flows of the propellers hitting the wing along a large portion of the wingspan.
The arrangement of the engines along the wing as described above is called DEP: Distributed Electric Propulsion.

## 1.1. DEP in general

DEP systems typically consist of different propeller configurations to exploit different aerodynamic effects:

- Boundary-Layer Ingestion: ducted fans or pusher propellers, typically installed at the tailcone or trailing edge of the wing, fill the wake, reducing the loss of kinetic energy and therefore drag.
- Wingtip propellers: Wingtip propellers rotate in the opposite direction to the wingtip vortices, reducing induced drag in the case of pulling propellers and increasing propeller efficiency in the case of pushing propellers due to the higher relative speed they encounter.

- High lift propellers: Propellers are positioned along the leading edge of the wing to increase the aerodynamic flow over the entire wing span, thereby increasing the resulting aerodynamic force and reducing the stall speed, allowing the design of a higher aspect ratio wing.
  The high lift propeller configuration is part of high lift systems and is generally not used during cruise.

Figure 1.1: NASA X-57 Maxwell [2].

Figure 1.1 shows the X-57 Maxwell, an aircraft designed by NASA to carry out several studies, including DEP propulsion.
High reliability, efficiency and low fuel consumption are the reasons driving research into DEP systems;
However, given the limited specific energy of batteries offered by current technology, an aircraft equipped with an full-electric DEP system is currently relegated to short-range missions.
However, a hybrid propulsion system would make it possible to solve this problem and extend the use of DEP systems to longer and more enduring missions, such as replacing narrow-body aircraft used to transport passengers or goods on regional routes.
DEP systems align well with electric propulsion due to the numerous benefits it offers, of which the most significant ones include:

- Scalability, which allows for the installation of multiple motors with lower power, without incurring additional weight.
- High efficiency.
- Greater energy density than conventional motors.

- There are no reductions in shaft power withincreasing altitude and airspeed.
- Low noise.
- Simplified maintenance.
- High reliability.

## 1.2. Aim and objectives

This thesis aims to extend Moretti's work [10] by creating a meta-model that includes the flap deflection as a parameter; This meta model is derived from simulations generated by typical ranges of parameters.
The meta-model will allow the estimation of the aeropropulsive interaction between the DEP system and the wing, even in configurations with extended flaps, and will allow these phenomena to be modelled more accurately than before.
This meta-model will be integrated into the TITAN algorithm, a program created by the Polytechnic of Milan, which is capable of performing preliminarily sizing of the aircraft.
In summary the main objectives of this thesis are:

- Compare new versions of OpenVSP to the one chosen by Moretti, in order to assess any advantages and disadvantages; This software is used to gather data for building the meta model.
- Construction of the meta model.
- Incorporation of the meta model into the already existing aircraft sizing routine.

## 1.3. Thesis outline

Chapter 2 evaluates different VLM software releases with the scope to identify suitable version, comparing the data obtained from these software with those validated by Moretti [10].
Chapter 3 uses a simple model equipped with plain flaps, to compare the behaviour obtained by varying the flap deflection by VLM simulations with a theoretical one.
Chapter 4 evaluates the increase in lift coefficient due to the DEP system for the UNIFIER19-C7A-HARW model at different flap deflections, obtained using Moretti's reduced method [10] and through two simulations: one simulation with all propellers running and one simulation with DEP system not working; so it's evaluated the error trend with flap deflection.
Chapter 5 proposes the numerical campaign adopted to create the meta-model and presents

the resulting increments in aerodynamic coefficients obtained.
Chapter 6 introduces the TITAN sizing routine and explains how the meta-model is integrated into it.
TITAN results obtained by using the meta-model with flaps, the meta-model without flaps and the results obtained without using any meta-model are commented.

# 2 | Numerical modelling

During the initial stage of design, utilising sophisticated numerical methods and highly defined models would be too time-consuming;
This is because multiple iterations are required for each flight configuration in the optimization process until optimal values are achieved.
As a result, these are the critical factors to consider when selecting the numerical methodology and refinement of the model.

## 2.1. Choice of the numerical method

There are many numerical methods that can be used to study aerodynamics, including:

- CFD has the highest accuracy, but it is unsuitable for this project phase due to its high computational cost.
- Patterson's method: Patterson employed the actuator disk theory to determine the dynamic pressure and AoA observed from the wing. This, in turn, allowed the determination of the sectional lift coefficient relative increment.
  Although this method tends to be conservative, in a preliminary stage this can be considered a good thing.
  De Vries used Patterson's method makes two simplifications; assuming a homogeneous flow on the wing and a sectional lift coefficient of $2\pi\alpha$.
  So, he devised an algebraic approach for determining also the DEP system's drag contribution [10].
- The Vortex lattice method (VLM) is a numerical approach that utilises a series of horseshoe vortices applied to a discretised lifting surface.
  This method can estimate the lift and induced drag with reasonable accuracy.
  Compared to the computational times required for CFD simulations, VLM is much faster, making it a practical choice for preliminary design phases.

The VLM method was selected for this thesis, in continuity with Moretti's work [10], over other numerical methods because of its computational costs and accuracy, which were

previously mentioned.
Consequently, this method will be discussed in greater detail below.
The VLM technique utilises the theory of thin profiles, therefore the wing profile is considered as a plate without thickness, which is discretised as shown in Figure 2.1.

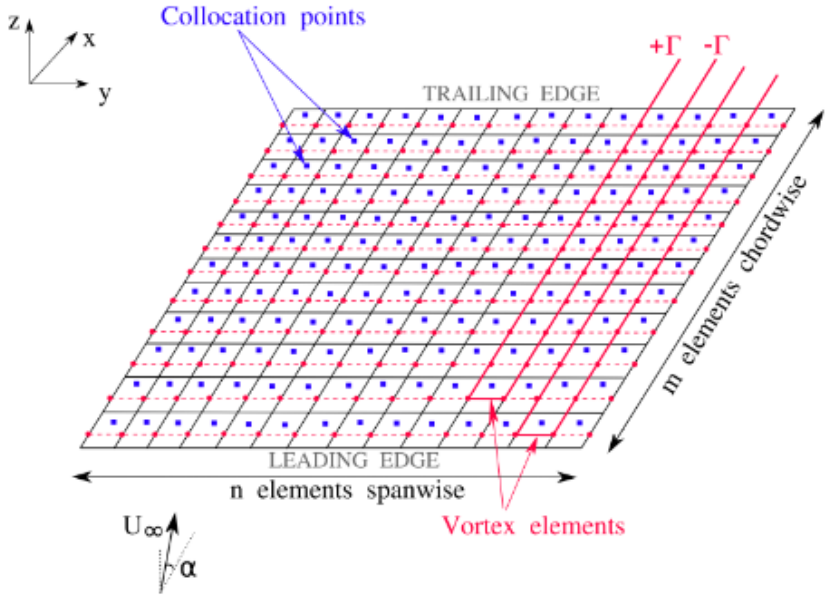


Figure 2.1: VLM discretization scheme [9].

Vortex intensity is determined by applying the non-penetration boundary condition at specific control points, also known as collocation points.
At these points, located at the three-quarter panel chord line, the flow in the direction of the panel's normal vector is prescribed to be zero.
Finally, the aerodynamic forces are determined by employing the Kutta-Joukowski theorem [7].
Propellers can be included in VLM simulations via two methods: Actuator disk theory and Purely VLM.
Actuator disk theory models thrusters as disks through which a specific airflow passes, calculated on the basis of thrust coefficients $C_T$ that are already known.
This method is less precise as it only considers the effect of the propeller on the wing, assuming a uniform flow in the disk area.
However, in the purely VLM approach, the propeller is modelled similarly to the wing, and an unsteady simulation is performed with the rotating propeller.
Furthermore, this method considers the effect of the propeller on the wing and vice versa.
Note that for this case, prior knowledge of the $C_T$ is not required; The only necessary

information is the RPM (revolutions per minute) at which the simulations are conducted. For conducting purely VLM simulations, the VSPaero program was utilised in this study; Developed by NASA, this open source software is included in the OpenVSP tool [8].

## 2.2. OpenVSP 3.23

Moretti validated [10] the OpenVSP 3.23 software using the models and experimental data obtained by Sinnige in his experiment [13].
In the following section, this data validation will be re-proposed to evaluate the possible use of a post 3.23 OpenVSP release.
Figure 2.2 displays the model representation.

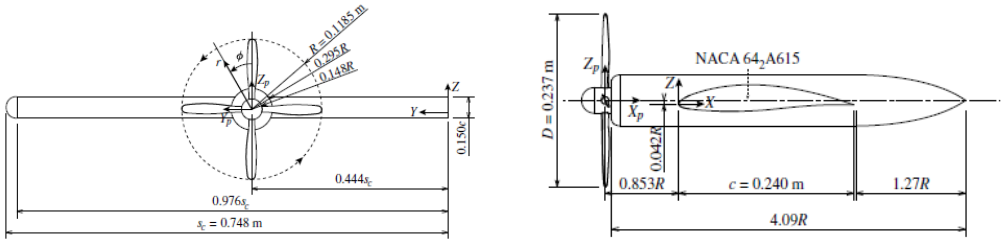


(a) Front view. (b) Lateral view.

Figure 2.2: Sinnige's experimental setup [13].

Of particular interest in Moretti's validation [10] is the fact that he had to change the hub radius from 15%R to 45%R in order not to incorrectly simulate the area of thick profiles, which are not suitable for simulation with a VLM method that has thin profiles among its hypotheses.
He also had to reduce the pitch of the blades by 2°, otherwise he would have found a deviation of the CT from that found experimentally, which is attributed to a low Reynolds number.
For the comparison of the OpenVSP versions in this thesis, the model developed by Moretti is used as a reference; To access additional insights and explorations on the validation of OpenVSP 3.23 carried out by Moretti, the reader is invited to refer to [10].

## 2.3. Other OpenVSP versions

As previously stated, NASA provides OpenVSP as an open source software, and it is regularly updated with new releases every few months.
At the time of writing this thesis the latest release available was the 3.33, which was

tested with the model validated by Moretti for the advance ratio value $J = 0.8$.
As can be seen in Figure 2.3 , the $C_L - \alpha$ curves in blown and unblown conditions have been overestimated.

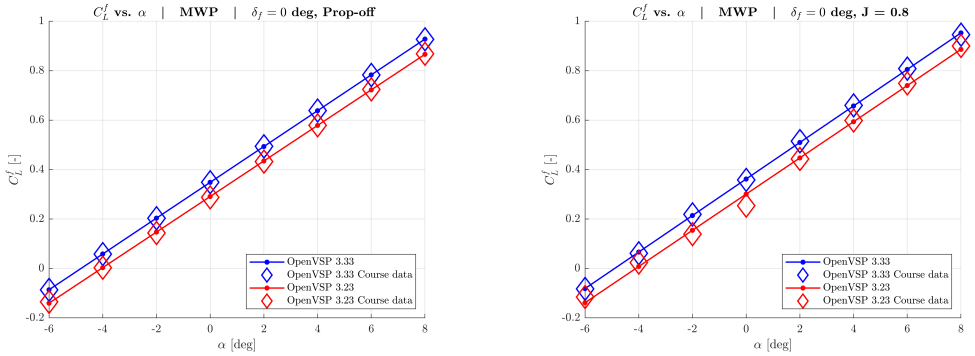


(a) $C_L - \alpha$ curve in prop-off condition. (b) $C_L - \alpha$ curve for $J = 0.8$.

Figure 2.3: Wing related lift coefficient comparison from OpenVSP 3.33 and OpenVSP 3.23.

This issue occurs because, as stated in [4], it is no longer feasible to modify the parameter $'a'$ in OpenVSP version 3.31 and later; Where $'a'$ represents: *"value which indicates the location along the chord where the chordwise loading changes from uniform to linearly decreasing toward the trailing edge"* [4].
From version 3.31, the value of this parameter remains constant at $a = 0.8$, which differs from the model used by Sinnige where $a = 1$.
We attempted to use the OpenVSP 3.30 version, with results shown in Figure 2.4 and Figure 2.5.

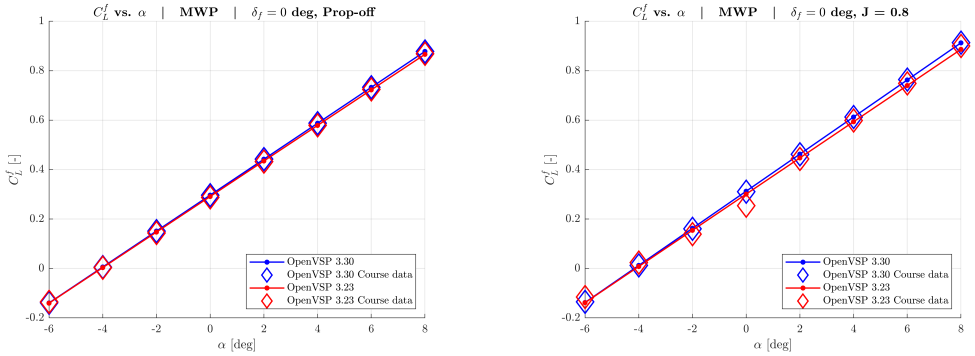


(a) $C_L - \alpha$ curve in prop-off condition. (b) $C_L - \alpha$ curve for $J = 0.8$.

Figure 2.4: Wing related lift coefficient comparison from OpenVSP 3.30 and OpenVSP 3.23.

Figure 2.4 demonstrate the correlation of the $C_L - \alpha$ curves with OpenVSP 3.23.

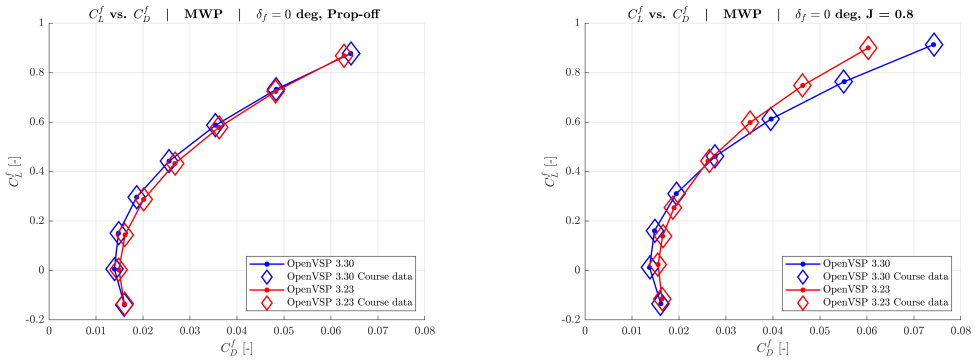


(a) Polar curve in prop-off condition.

(b) Polar curve for $J = 0.8$.

Figure 2.5: Wing related polars comparison from OpenVSP 3.30 and OpenVSP 3.23.

With the OpenVSP version 3.30, there is a discrepancy in the $C_{D0}$ and k values of the analytical drag Equation 2.1 discovered in both blown and unblown cases, which can be observed in Figure 2.5.

$$C_D = minC_{D0} + K(C_L - C_{L,min_{CD}})^2 \tag{2.1}$$

Furthermore, a higher $C_T$ is achieved compared to the reference value for that particular $J$ value.
Due to these considerations, it was decided to keep OpenVSP 3.23 version for the study of this thesis.

# 3 | Flapped wing aerodynamics

Improving the meta model by incorporating flaps constitutes the primary objective of this thesis; Therefore, examining their response through VLM simulations and comparing the results with the theory expected behaviour is important.
In order to examine the behaviour of VLM simulations with varying flap deflection, the Sinnige model was selected due to its simplicity.
The model of the previous section was adapted by incorporating Plain flaps, the type intended for the meta-model; The flaps also have a dimensionless value $c_f/c = 0.25$, which is consistent with the model used to construct the meta-model.
The flaps were positioned along the entire wing span to simplify the aerodynamic response.

## 3.1. Theoretical framework

Reference [12] outlines the aerodynamic behaviour of wings with the addition of three types of flaps: plain flap, slotted flap, and extending flap.
Plain flaps increase the wing's camber, which in this way shifts the CL-alpha curve upwards without changing its slope.
Slotted flaps include a slot in the flap hinge to allow high pressure air to pass over the top of the flap, energising the airflow and delaying the stall angle.
For the extending flap [12] reported that: *"The wing area is increased as the flap deflects, so the wing generates more lift at any given angle of attack compared to the non-extending flap.*
*Because the lift coefficient is referenced to the original wing area, not the extended wing area, the effective slope of the lift curve for an extending flap is increased by approximately the ratio of the total extended wing area to the original wing area".*
Increasing the total wing area therefore increases the lift force:

$$L_{flap} = qSC_L = qS_fCL' > L_{clean}, \tag{3.1}$$

From Equation (3.1) it's obtained:

$$C_L = \frac{S_f}{S} C'_L, \tag{3.2}$$

$$C_{L0} + C_{L\alpha}\alpha = \frac{S_f}{S}(C'_{L0} + C'_{L\alpha}\alpha), \tag{3.3}$$

When we equalise the first degree components of the polynomial from Equation (3.3), it becomes evident, as reported by [12], that extending flaps increases the slope. This occurs due to the ratio between the total wing area with flaps extended and the original wing area.
An increase in the $C_{L0}$ value is observed when the total wing area with flaps extended to the clean configuration wing area ratio is increased.
The introduction of the DEP system creates an effective dynamic pressure greater than the reference one, as the airflow passing through the propellers is energised and has a speed greater than the airspeed of the aircraft.
It is found that the aerodynamic effect of the DEP system resembles that of the extending flaps, as shown by Equations (3.4) and (3.5):

$$L_{DEP} = qSC_L = q_e SCL' > L_{clean}, \tag{3.4}$$

$L_{DEP}$ represents the lift generated with the DEP system in operation, while $q_e$ is the effective dynamic pressure which takes into account the actual flow speed with the DEP system active.
From Equations (3.4) it's obtained:

$$C_L = \frac{q_e}{q} C'_L, \tag{3.5}$$

Equation (3.5) closely resembles Equation (3.2), but with the ratio of dynamic pressures in place of the ratio of wing surfaces.
Also in this instance, we can anticipate an increase in $C_{L\alpha}$ and $C_{L0}$ through the correlation between the effective dynamic pressure and the reference one.
The expected result of using both the DEP system and the plain flaps is the sum of their individual effects, therefore $C_{L0}$ will increase due to the use of the DEP system and the plain flaps, and $C_{L\alpha}$ will increase as a result of the DEP system.

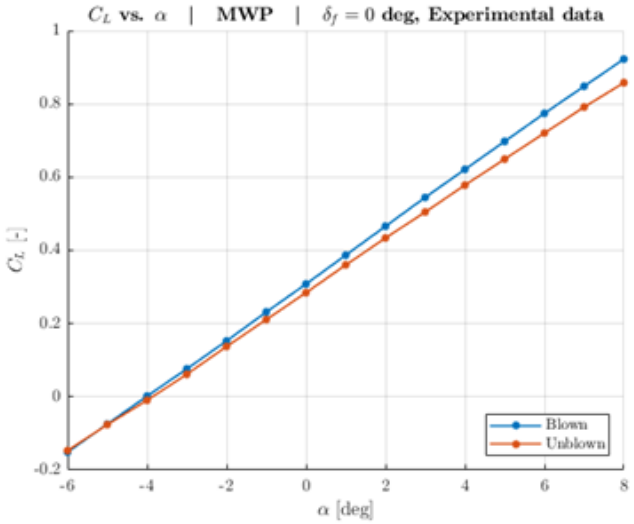


Figure 3.1: $C_L - \alpha$ curve obatained from Sinnige's experimental data [13].

To compare the isolated effect of the DEP system with that hypothesised above, Figure 3.1 displays the Sinnige's experimental results without flaps, after thruster data reduction. The data show a linear trend in both unblown and blown cases in the $C_L - \alpha$ curves; Additionally, an increase in $C_{L0}$ and $C_L - \alpha$ is reported, highlighting the hypothesized trend.

An important factor concerning the flaps is the derivative of the lift coefficient in relation to the flap deflection; This coefficient is commonly referred to as flap effectiveness, as it indicates the sensitivity of $C_L$ to the varying deflection of the flaps.

Reference [12] provides Equation (3.6) for computation of the derivative described above:

$$C_{L,\delta f} = 0.9 K_f C_{l,\delta f} \frac{S_f}{S} \cos \Lambda_{H.L.}, \tag{3.6}$$

Equation (3.6) comprises the sectional lift coefficient of the flaps derivatives $C_{l,\delta f}$, the cosine of the sweep angle of the flap hinge line $\cos \Lambda_{H.L.}$, the flapped wing and wing surface; These parameters remain constant regardless of the deflection of the flaps.

Equation (3.6) also comprises the correction factor $K_f$, found empirically, which instead varies with the deflection of the flaps and the $c_f/c$ coefficient.

As $K_f$ is the only term that varies with the flap deflection, the $C_{L,\delta f}$ term must have the same trend as this coefficient, reported in Figure 3.2.

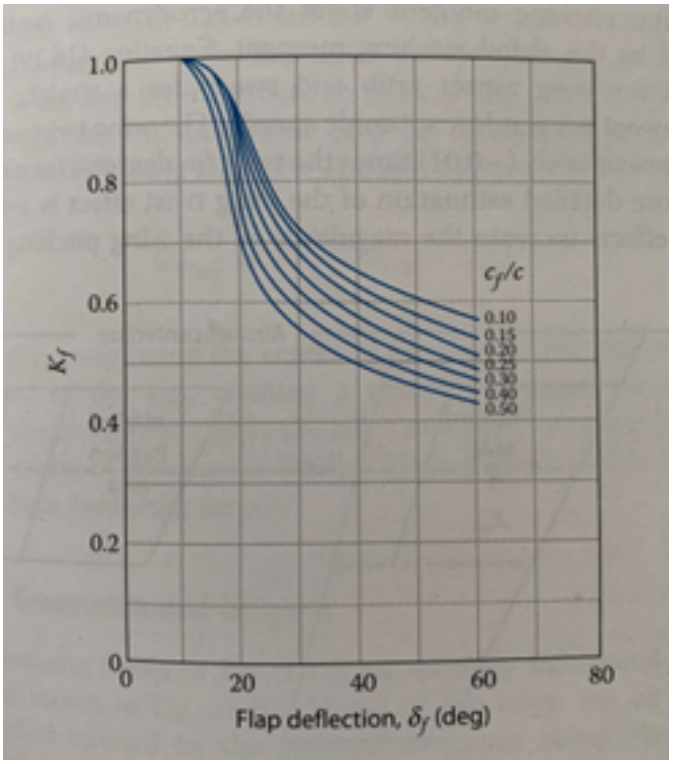


Figure 3.2: Plain Flap correction factor $K_f$ [12].

## 3.2. Model description

The Sinnige's model [13] used in Section 2.3 to confront the OpenVSP versions is now used to study the aerodynamics with flap deflection.
Table 3.1 and 3.2 report wing and propellers parameter of this model.

| | Value |
|---|---|
| $b$ | 1.46 m |
| $\overline{c}$ | 0.24 m |
| $S$ | 0.35 $m^2$ |
| $AR$ | 6.08 |
| $\Lambda$ | 0° |
| $\lambda$ | 1 |
| $\Gamma$ | 0° |
| $\alpha_t$ | 0° |
| $i_w$ | 0° |
| Airfoil | NACA 64A615, a=1.0 |
| $(t/c)_r$ | 0.15 |
| $(t/c)_t$ | 0.15 |

Table 3.1: Wing geometry parameters for Sinnige's model.

| | Value |
|---|---|
| $d$ | 0.237 m |
| $r_h$ | 0.107 m |
| $\beta_{3/4}$ | 21.9° |
| $\epsilon$ | 0° |

Table 3.2: Sinnige's model propellers parameter [10].

As can be seen from the Figure 3.3, this model has been fitted with plain flaps along all the wing spanwise and with a flap chord to wing chord ratio of 0.25, these parameters are reported in Table 3.3; Refer to Section 4.2 and Figure 4.1 for flap parameters description.

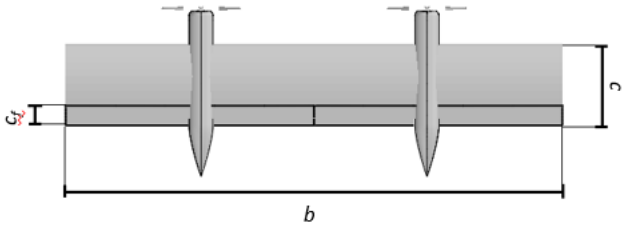


Figure 3.3: Sinnige's model fitted with flaps.

| | **Value** |
|---|---|
| $H_I$ | 0 [-] |
| $H_O$ | 1 [-] |
| $Cf/C$ | 0.25 [-] |

Table 3.3: Settled flap parameters.

Simulation with this model is carry on for the single value of $J$ equal to 0.8.

## 3.3. Results

Initially, the trend of the $C_L - \alpha$ curves is examined in the unblown scenarios, to observe the flap deflection effect without the DEP system working.
According to [12], a first estimation shows an upward shift of the $C_L - \alpha$ curve with flap deflection, with no change in its slope, as shown in Figure 3.4 and 3.5,

According to [12], flap deflection leads in a first estimation to an upward shift of the $C_L - \alpha$ curve, with no change in its slope, as shown in Figure 3.4;
A first evaluation of Figure 3.5 confirms this estimation.

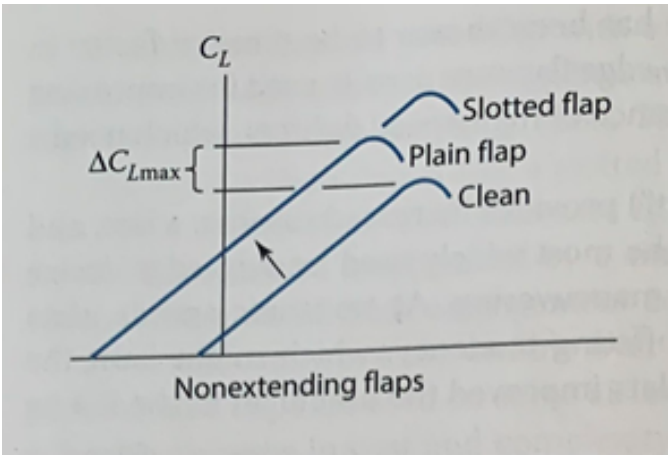


Figure 3.4: Approximate Flaps effect [12].

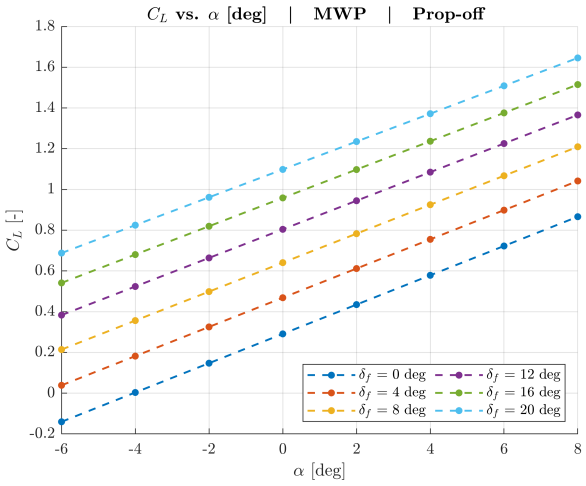


Figure 3.5: $C_L - \alpha$ unblown curves.

Table 3.4 allows for detailed examination of the slope of the $C_L - \alpha$ curve achieved via the VLM method with propellers not working, indicating a slight decrease in slope when flaps deflect.
It is assumed that this phenomenon is due to the increase of the extremity vortices intensity with increasing of the wing camber due to the flap deflection.

| $\delta_f$ [°] | 0 | 4 | 8 | 12 | 16 | 20 |
|---|---|---|---|---|---|---|
| $C_{L,\alpha}$ [-] | 0.0719 | 0.0716 | 0.0711 | 0.0702 | 0.0695 | 0.0684 |

Table 3.4: $C_{L,\alpha}$ with flap deflection, obtained by OpenVSP with propellers not working.

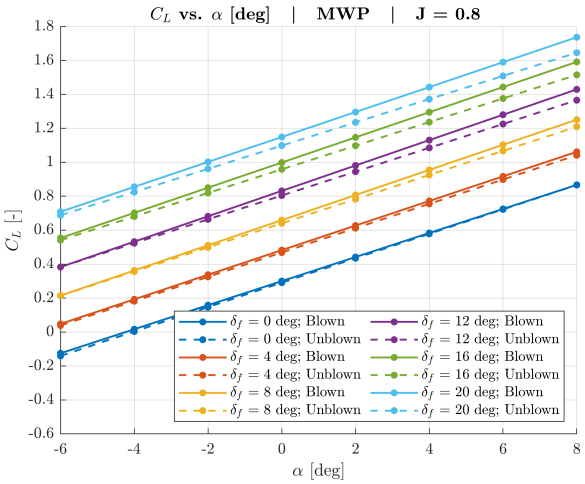


Figure 3.6: $C_L - \alpha$ curves with $J = 0.8$.

Figure 3.6 compares the $C_L - \alpha$ curves in the blown and unblown cases.
The trend of the individual linear coefficients will be evaluated later; however, it is immediately apparent that the slope increases with the deflection of the flaps, as previously predicted.
To obtain this coefficients, separate linearizations were performed for each flap deflection value in both the blown and unblown cases.

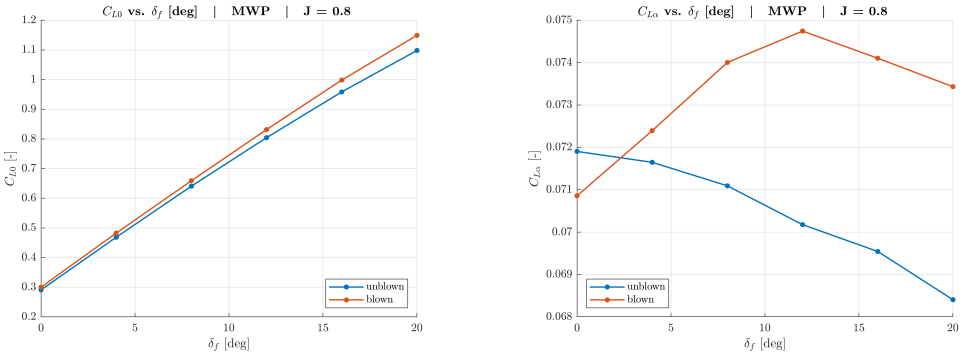


(a) $C_{L0} - \delta_f$ curve for prop-off and $J = 0.8$. (b) $C_{L\alpha} - \delta_f$ curve for prop-off and $J = 0.8$.

Figure 3.7: Linear coefficient behavior.

Figures 3.7a and 3.7b show the trend of the $C_{L0}$ and $C_{L\alpha}$ coefficients as the flap deflection varies.
In Section 3.1, for the unblown case, it was hypothesised an increase in $C_{L0}$ with flap deflection and it is confirmed by Figure 3.8a.
As previously shown in Table 3.4, in the unblown case the $C_{L\alpha}$ coefficient exhibits a de-

creasing trend, which is attributed to the increased intensity of tip vortices.
For the blown case, Section 3.1 hypothesised that the combined effect of the DEP system and plain flaps would result in additional increases in both $C_{L0}$ and $C_{L\alpha}$ with flaps deflection.
Even for the blown case, Figure 3.7a reflects what is expected according to the theory, with the $C_{L0}$ curve increasing and being higher than that of the unblown case.
The $C_{L\alpha}$ curve has a first increasing phase, as expected by the theory, and a second decreasing phase, which is hypothesized due to the predominant effects of the tip vortices.

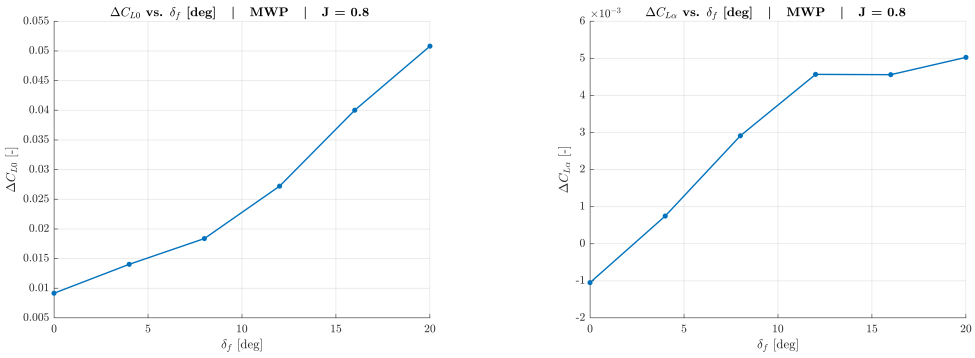


(a) $\Delta C_{L0} - \delta_f$ curve for prop-off and $J = 0.8$ condition.

(b) $\Delta C_{L\alpha} - \delta_f$ curve for prop-off and $J = 0.8$.

Figure 3.8: Blown and unblown linear coefficient gap.

Figures 3.8a and 3.8b show the difference between the linear coefficients of the blown cases and those of the unblown cases;
The trend of $\Delta C_{L0}$ is not too far from the linearity hypothesised in the theory; $\Delta C_{L\alpha}$ curve has an approximately linear trend in a first phase, which flattens out in a second phase due to the increased intensity of the tip vortices.
The sensitivity of $C_L$ to varying flap deflection is indicated by an important parameter known as flap effectiveness, which is the derivative of $C_L$ with respect to flap deflection. $C_{L,\delta_f}$ is computed by central derivatives and left and right derivatives at the extremes of the flap deflection interval.

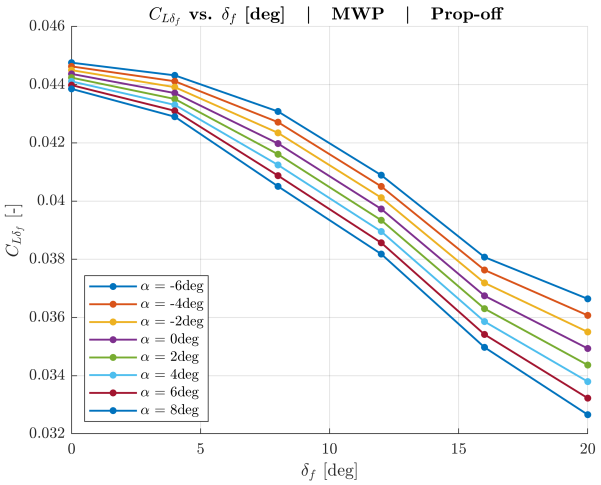


Figure 3.9: $C_{L,\delta_f} - \delta_f$ curves for prop-off case.

Figure 3.10 shows the $C_{L,\delta_f}$ obtained for every $\alpha$ and $\delta_f$ values in the unblown cases; The trend of these curves corresponds to the theoretical one proposed in Section 3.1 in Figure 3.2, which confirms the validity of the results obtained with the VLM method with flaps deflected.

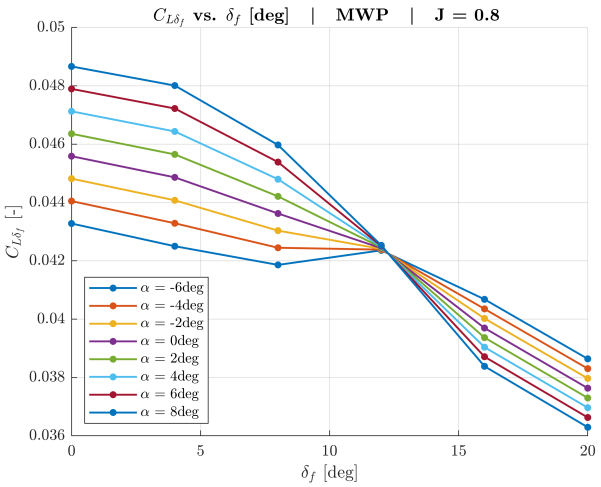


Figure 3.10: $C_{L,\delta_f} - \delta_f$ curves for $J = 0.8$.

Figure 3.10 presents the behavior of the $C_L$ derivative with flaps in the blown case.
The curves with the angle $\alpha$ between -6° to -2° exhibit a peak at $\delta_f = 12$.
This can be attributed to the $C_{L\alpha}$ coefficient which shows an upward trend until $\delta_f = 12$ and thereafter decreases with the flap deflection, reaching a maximum at this point, as presented in Figure 3.7b.
As demonstrated by the Equation (3.7), the $C_{L\alpha}$ increasing trend is asociated with a

$\frac{\partial C_{L\alpha}}{\partial \delta_f} > 0$ and it has a negative impact on the $C_{L,\delta_f}$ coefficient for negative alphas, but has a positive effect when the $C_{L\alpha}$ trend is decreasing and the alphas are negative.

$$C_{L,\delta f} = \frac{\partial C_{L0}}{\partial \delta_f} + \frac{\partial C_{L\alpha}}{\partial \delta_f}\alpha, \tag{3.7}$$

The contribution of the $C_{L\alpha}$ on $C_{L,\delta_f}$ is minor and not sufficient to change the sign of the $C_{L,\delta_f}$ coefficient, but it creates that maximum point.
The $C_{L,\delta_f}$ curves for $\alpha$ angles ranging from 0° to 8° exhibit the anticipated behaviour concerning the unblown case. This is due to the fact that the contribution given by $C_{L0}$ undergoes variations as the deflection of the major flaps changes. The contribution given by $C_{L\alpha}$, however, is affected to a lesser extent.

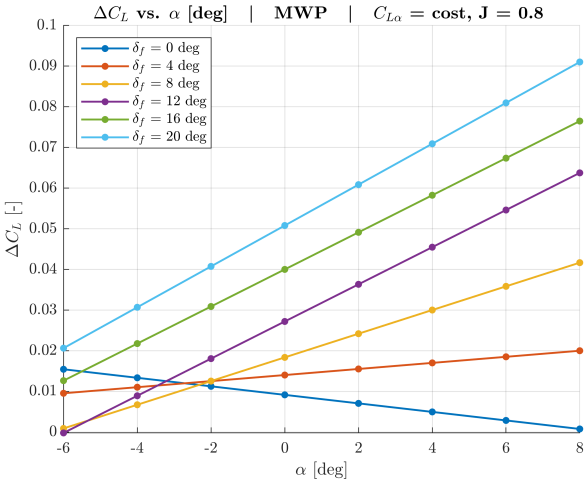


Figure 3.11: $\Delta C_L - \alpha$ curves blown and unblown gap.

Figure 3.11 illustrates the $\Delta C_L$ curves, which result from subtracting unblown case $C_L - \alpha$ curves from those with propellers in operation.
These curves are derived by calculating the difference in $C_L$ between the blown and unblown cases presented in Figure 3.6 and 3.5, consequently they reflect all the previous analyses.
This chapter presented an analysis of the aerodynamic behaviour with flaps deflection, using the Purely VLM method.
The results demonstrate limited deviations from the expected behaviour.
Therefore, it is assumed that the pure VLM method with the adopted software is suitable for modelling the wing even when equipped with Plain Flap high-lift devices.

# 4 | Application to UNIFIER19

In his thesis [10], Moretti selected the UNIFIER19 as the basis for constructing the meta-model.
This aircraft was designed by Politecnico di Milano in partnership with Pipistrel, and was chosen due to the availability of pre-existing models and comprehensive geometry information suitable for OpenVSP.

## 4.1. Aircraft description

The UNIFIER19 is a hybrid-electric commuter intended to replace current airplanes in the same category with its near-zero-emission model.
Several designs have been created throughout the years. The version used in this thesis and in Moretti's is the C7A-HARW, where HARW stands for High Aspect Ratio Wing, in fact the aspect ratio of the wing has been increased from 9 to 14.
Other fundamental characteristics of the wing, whose values are presented in the Table 4.1, are a pronounced taper, slightly negative dihedral and twist, and a thickness ratio variable spanwise.

| | Value |
|---|---|
| $b$ | 20.11 m |
| $\bar{c}$ | 1.54 m |
| $S$ | $28,90$ m$^2$ |
| $AR$ | 14 |
| $\Lambda$ | 0° |
| $\lambda$ | 0.37 |
| $\Gamma$ | $-2°$ |
| $\alpha_t$ | $-3°$ |
| $i_w$ | 3° |
| Airfoil | LS(1)-0413 MOD |
| $(t/c)_r$ | 0.195 |
| $(t/c)_t$ | 0.129 |

Table 4.1: UNIFIER19-C7A-HARW's wing geometry parameters.

The propeller models are the ones of the C7A-HARW configuration, and all relevant parameter values are provided in Table 4.2.

| | Value |
|---|---|
| $d$ | 1.6 m |
| $r_h$ | 0.163 m |
| $\beta_{3/4}$ | 31.5° |
| $\epsilon$ | $-5°$ |

Table 4.2: UNIFIER19-C7A-HARW's HLP parameters.

Since the DEP system is not used during the cruising phases, HLPs offer folding and unfolding configurations, falling back to reduce aerodynamic resistance.
In the C7A-HARW configuration there are 12 identical propellers, positioned on the leading edge and uniformly distributed along the wingspan, with zero separation between the blades, to increase the blown surface without having overlaps; The Table 4.3 illustrates the relative position of propellers in relation to the wing semispan.

| | $Prop_1$ | $Prop_2$ | $Prop_3$ | $Prop_4$ | $Prop_5$ | $Prop_6$ |
|---|---|---|---|---|---|---|
| $\|Y\|$ | 2.05 m | 3.65 m | 5.25 m | 6.85 m | 8.45 m | 10.05 m |

Table 4.3: HLP's spanwise position for UNIFIER19-C7A-HARW [10].

## 4.2. Flap description

The UNIFIER19 aircraft model has already been fitted with Plain Flaps and they have not been modified. These type of flaps are straightforward in construction, equipped with a hinge that enables rotation for deflection. The parameters for these flaps are detailed in Table 4.4, where the $H_I$ is the starting point of the flaps with respect to the wing span, the $H_O$ is the outer point of the flaps with respect to the span, the $SwfS$ is the ratio of the flapped wing area to the wing area.
When $H_I$ and $H_O$ are selected, the $SwfS$ is fully defined.
$c_f/c$ is the ratio of flap chord to wing chord.
Figure 4.1 displays these values.

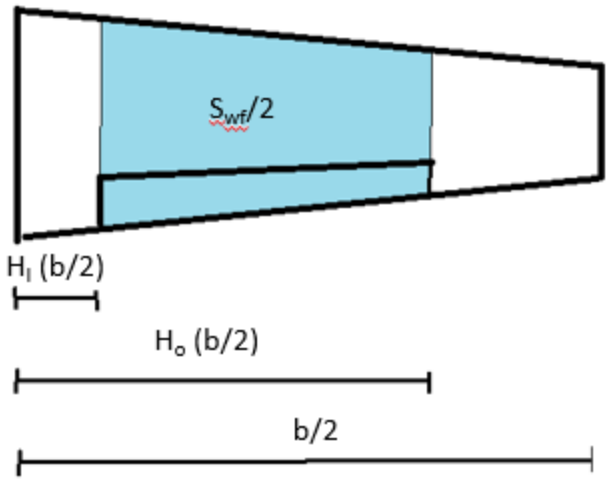


Figure 4.1: Flap parameters scheme.

| | Value |
|---|---|
| $H_I$ | 0.11 [-] |
| $H_O$ | 0.8 [-] |
| $SwfS$ | 0.72 [-] |
| $Cf/C$ | 0.25 [-] |

Table 4.4: UNIFIER19 flaps characteristics.

The $c_f/c$ remains constant along the span, Section 5.1 will demonstrate that this ratio is one of the dimensionless groups describing the aeropropulsion model, so a constant value is the simplest way to characterise the model;
Furthermore, when this ratio is constant, the flap chord varies linearly along the span, allowing the use of the reduced method during data acquisition, which requires linear parameter variation along the spanwise.
The benefits of use Plain Flap are:

- Simplicity of construction and design.
- Low production costs.

The disadvantages of using these type of flaps are:

- The area of the flap remains constant with the deflection (non-extendable flaps); The use of extendable flaps could increase the lift offered by the flaps.
- When deflection angles exceed 30°, flow separations occur at the flaps; in the case of slotted flaps, the air flow is energised, reducing the separation phenomenon [12].

The plain flaps deflection results in the upward translation of the $C_L - \alpha$ curve without altering its slope, this occurs since the deflection only affects the wing mean line curvature but not the wing surface.

## 4.3. Moretti's method: Simple wing

Due to the high number of iterations that the sizing phase involves, performing unsteady simulations with the pure Vortex Lattice Method (VLM) requires a significant investment of timing code.
For this reason, it was decided to perform these simulations outside the Titan routine, in order to perform them only once for an expected range of parameters.

For every flap value, 54 test points are required to cover the typical parameter range chosen by Moretti in his work [10].
To decrease computational effort, Moretti found a reduced method that required 4 simulations for each test point, instead of one simulation for each propeller and a specific simulation for the wing without propellers.
Taking advantage of the linear variation of the wing parameters along the span, Moretti assumed and verified, as shown in Figure 4.2, that the lift and drag increments produced by the contribution of each pair of propellers positioned along the span also vary linearly along the span.

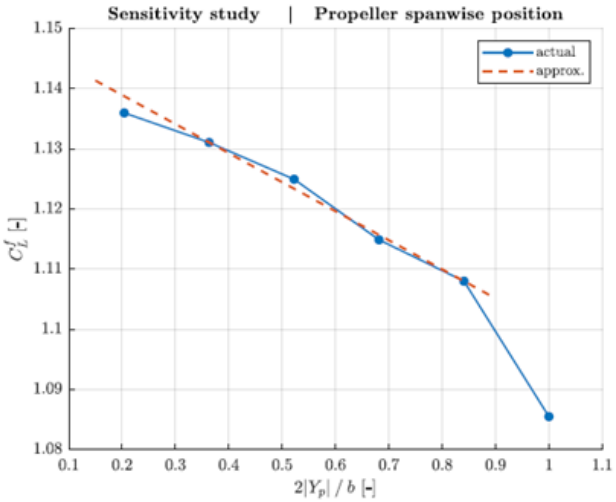


Figure 4.2: Moretti's plot [10]: Lift coefficient sensitivity to propeller spanwise position for UNIFIER19 in configuration C7A-HARW.

Figure 4.2 demonstrates the linear relationship of $C_L$ values obtained with only the pair of propellers located at a specific position on the wingspan present in the simulation.
Therefore, these $C_L$ values can be approximated linearly along the span, except for the WTPs, which operate on a comparatively smaller wing surface than the other thrusters.
In this approach, the $C_L$ is considered to be the sum of $C_{Lu}$ and $\Delta C_L$.
The Equations (4.1) obtained from [10], applicable to simulations with $Prop_2$, $Prop_5$, or both, are utilised for computing $\Delta C_{L2}$, $\Delta C_{L5}$ and $C_{Lu}$.

$$\begin{cases} C_{Lu}^f + \Delta C_{L2}^f = C_{L2}^f \\ C_{Lu}^f + \Delta C_{L5}^f = C_{L5}^f \\ C_{Lu}^f + \Delta C_{L5}^f + \Delta C_{L5}^f = C_{L2\&5}^f \end{cases} \tag{4.1}$$

If further information on this method is desired, the reader is directed to refer to [10].
In his thesis, Moretti verified that the results obtained with the reduced method were the approximate values of those obtained with a single simulation with all 12 propellers present and a simulation without propellers.

## 4.4. Extension to Moretti's method: Flapped Wing

Adding flap deflection to the parameters requires 54 test points for each flap deflection value maintaining the same range of the other parameters.
Due to the selection of four flap deflection test points ranging from 0° to 30°, the construction of the meta model necessitated 216 test points.
The significance of reducing the computational cost is evident.
To illustrate that even with deflected flaps, a reduced approach is still feasible, simulations of the UNIFIER19 model were conducted with an AoA of 4° and flap deflection at 0°, 10°, and 20°.

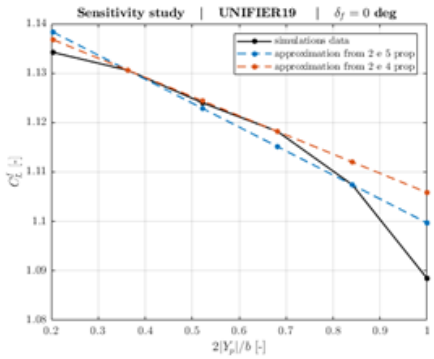


(a) $\delta_f = 0°$.

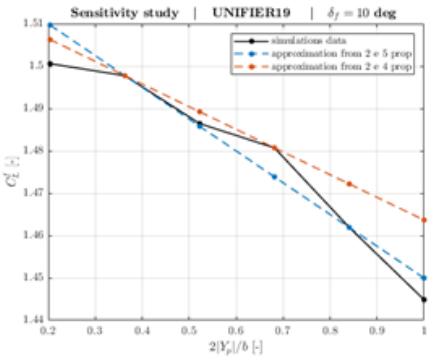


(b) $\delta_f = 10°$.

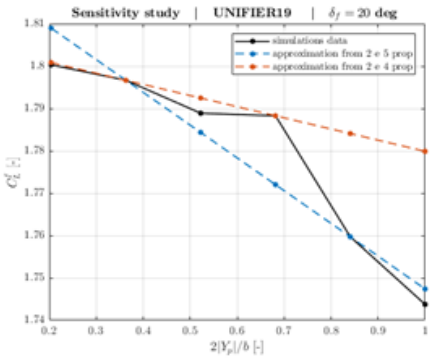


(c) $\delta_f = 20°$.

Figure 4.3: Lift coefficient sensitivity to propeller spanwise position for UNIFIER19 configuration C7A-HARW, for different flap deflections.

As shown in Figures 4.3, when the flaps are deflected, the coefficient of lift can be linearly approximated along the spanwise position with only one pair of propellers present.
However, this approximation is only valid from $Prop_1$ to $Prop_4$ and not to $Prop_5$.
Despite the flap deflection, $Prop_1$ to $Prop_4$ still operate on a portion of the wing surface where its parameters change linearly along the wingspan, hence $C_L$ and $C_D$ preserve this linearity property; on the other hand, $Prop_5$ operates on a part of the wingspan outside the flaps, and therefore on a part of the wing with a lower camber angle.
Positioned at the wing tips, the WTPs act on both a wing section not covered by the flaps and a on a lower wing surface.
Table 4.5 present $C_L$ and $C_D$ values obtained from a single simulation at $\delta_f = 0°$ with all propellers included, alongside those obtained through reduced methods from $Prop_1$ to $Prop_5$ and $Prop_1$ to $Prop_4$.

| | $C_{L,AllProp}$ | $C_{D,AllProp}$ | $C_{L,red24}$ | $C_{D,red24}$ | $C_{L,red25}$ | $C_{D,red25}$ |
|---|---|---|---|---|---|---|
| **Blown** | 1.3497 | 0.1115 | 1.3388 | 0.1075 | 1.3534 | 0.1051 |
| **Unblown** | 1.0491 | 0.0809 | 1.0734 | 0.0824 | 1.0699 | 0.0828 |

Table 4.5: Numerical results for $\delta_f = 0°$.

Tables 4.6 and 4.7 reports the lift and drag coefficient for the flap-deflected configurations. These values were obtained through a simulation with all propellers operating and from the reduced method between $Prop_1$ and $Prop_4$.
As the flap deflection causes a loss of linearity in the increase of lift coefficient with respect to $Prop_1$ to $Prop_4$, the reduced method was not assessed for these configurations by linearizing from $Prop_1$ to $Prop_5$.

| | $C_{L,AllProp}$ | $C_{D,AllProp}$ | $C_{L,red24}$ | $C_{D,red24}$ |
|---|---|---|---|---|
| **Blown** | 1.7415 | 0.1552 | 1.7342 | 0.1488 |
| **Unblown** | 1.4283 | 0.1112 | 1.4293 | 0.1146 |

Table 4.6: Numerical results for $\delta_f = 10°$.

| | $C_{L,AllProp}$ | $C_{D,AllProp}$ | $C_{L,red24}$ | $C_{D,red24}$ |
|---|---|---|---|---|
| **Blown** | 2.0610 | 0.2027 | 2.0354 | 0.1979 |
| **Unblown** | 1.7543 | 0.1461 | 1.7293 | 0.1505 |

Table 4.7: Numerical results for $\delta_f = 20°$.

Tables 4.8 and 4.9 shows the errors related to the previous quantities; the relative errors are calculated according to the Equation (4.2):

$$e_{rel,CL} = \frac{C_{L,red} - C_{L,AllProp}}{C_{L,AllProp}}, \tag{4.2}$$

The reference value used to calculate the relative error is the coefficient obtained from simulations with all propellers or with no propeller.
In both blown and unblown cases with undeflected flaps, the $C_L$ obtained using the reduced method between $Prop_1$ and $Prop_4$ display comparable but slightly greater errors than those obtained using the reduced method between $Prop_1$ and $Prop_5$.
Furthermore, the case with $\delta_f = 0°$ shows an underestimation of the $C_L$ in blown condition and an overestimation of the $C_{Lu}$, giving the reduced method between $Prop_1$ and $Prop_4$ more conservatism in the calculation of $\Delta C_L$, which is favourable in a preliminary design phase.

| | $err_{CL,red24}$ [-] | $err_{CD,red24}$ [-] | $err_{CL,red25}$ [-] | $err_{CD,red25}$ [-] |
|---|---|---|---|---|
| **Blown** | -0.0109 | -0.0040 | 0.0027 | -0.0569 |
| **Unblown** | 0.0243 | 0.0015 | 0.0198 | 0.0229 |

Table 4.8: Errors in Numerical results for $\delta_f = 0°$.

| | $err_{CL,red24}$ [%] | $err_{CD,red24}$ [%] | $err_{CL,red25}$ [%] | $err_{CD,red25}$ [%] |
|---|---|---|---|---|
| **Blown** | -0.8 | -3.6 | 0.27 | -5.7 |
| **Unblown** | 2.3 | 1.8 | 2 | 2.3 |

Table 4.9: Relative errors in Numerical results for $\delta_f = 0°$.

The tables below present the errors for $\delta_f = 10°, 20°$; No increase in errors was observed resulting from flap deflection.

| | $err_{CL,red24}$ [-] | $err_{CD,red24}$ [-] |
|---|---|---|
| **Blown** | -0.0073 | -0.0064 |
| **Unblown** | 0.0010 | 0.0034 |

Table 4.10: Errors in Numerical results for $\delta_f = 10°$.

| | $err_{CL,red24}$ [%] | $err_{CD,red24}$ [%] |
|---|---|---|
| **Blown** | -0.42 | -4.12 |
| **Unblown** | 0.07 | 3.08 |

Table 4.11: Relative errors in Numerical results for $\delta_f = 10°$.

| | $err_{CL,red24}$ [-] | $err_{CD,red24}$ [-] |
|---|---|---|
| **Blown** | -0.0256 | -0.0048 |
| **Unblown** | -0.0250 | 0.0044 |

Table 4.12: Errors in Numerical results for $\delta_f = 20°$.

| | $err_{CL,red24}$ [%] | $err_{CD,red24}$ [%] |
|---|---|---|
| **Blown** | -1.24 | -2.39 |
| **Unblown** | -1.43 | 3.02 |

Table 4.13: Relative errors in Numerical results for $\delta_f = 20°$.

It was therefore decided to continue using the Moretti's reduced method, linearising the increase in $C_L$ and $C_D$ resulting from the contribution of the propellers from $Prop_1$ to $Prop_4$, and to run separate simulations to calculate the contribution of $Prop_5$ and WTP.

# 5 | Implementation of meta-model

This chapter presents the development of a meta model for predicting aero-propulsive interaction between the DEP system and the wing.
By constructing the meta model outside of TITAN code via a dedicated numerical campaign, various advantages are realized.
Firstly, computational costs are incurred only once during the construction of the meta model since TITAN accesses this database when it is necessary during the sizing phase.
The TITAN code's structure enables the algorithm to operate with or without a meta model.
Furthermore, the code's modular structure enables easy adjustments of specific modules, leading to a more efficient and simplified process.
Additionally, modular design offers the most straightforward approach to enhancing the precision of the meta model by adding new parameters, as demonstrated in this thesis.

## 5.1. Dimensional analysis

The initial stage of model development revolves around identifying parameters that are independent of one another, and thus capable of describing all degrees of freedom.
To do this, the Buckingham's Π theorem was applied, following the procedure used by Moretti [10], with the introduction of additional parameters to take into account the flaps. Buckingham's Π theorem, applied to achieve this aim, state that: *"if a quantity Q0 (a dependent variable) is completely determined by the values of a set of n independent quantities, of which a number k form a complete, dimensionally independent subset, then a suitable dimensionless Q0 will be completely determined by n – k dimensionless similarity parameters"* [14].
The function of a generic aeropropulsive force on a flapped wing is the following:

$$F = F(\rho, a, \mu, V, \alpha, S, \epsilon, d, N, S_{wf}, \delta_f, c_f) \tag{5.1}$$

The force is therefore assumed to depend on the density of the air ($\rho$), the speed of sound

($a$), the viscosity of the air ($\mu$), the flight speed ($V$), the angle of attack ($\alpha$) , the wing surface area ($S$), the propeller tilt angle with respect to the wing chord ($\epsilon$), the propeller diameter ($d$), the propeller RPM ($N$), the flapped wing area ($S_{wf}$) and the flap deflection ($\delta_f$).
Eq.5.1 indicates that there are $n = 12$ variables describing the system and $k = 3$ fundamental dimensions (mass, length and time); Among the system variables, $\alpha$, $\epsilon$, and $\delta_f$ are already dimensionless and consequently belong to the dimensionless groups.
The first dimensionless group is the force coefficient, the quantity to be determined:

$$\pi_1 = \frac{F}{\rho V^2 S} = C_F \tag{5.2}$$

The second dimensionless group is the Mach number:

$$\pi_2 = \frac{V}{a} = M \tag{5.3}$$

The third dimensionless group is the Reynolds number:

$$\pi_3 = \frac{\rho V \sqrt{S}}{\mu} \approx Re \tag{5.4}$$

The Reynolds number requires the chord of the airfoil to be used as the characteristic length in the case of airfoils.
However, Titan employs a constant aspect ratio, which is chosen in the input file. Consequently, with constant aspect ratio, the reference length $\sqrt{S}$ is proportional to the mean aerodynamic chord of the wing; Consequently, the third dimensionless group will also be proportional to the Reynolds number.
The fourth dimensionless group is determined by the ratio of the diameter of the propeller to the square root of the wing area, the diameter of the propeller represents its characteristic length:

$$\pi_4 = \frac{d}{\sqrt{S}}\ r_p \tag{5.5}$$

The fifth dimensionless group can be seen as the product of the dimensionless group $r_p$ and the dimensionless number advance ratio $J$:

$$\pi_5 = \frac{V}{N\sqrt{S}} = Jr_p \tag{5.6}$$

The sixth dimensional group is given by the ratio between the flapped wing surface and the wing surface:

$$\pi_6 = \frac{S_{wf}}{S} = SwfS \tag{5.7}$$

The seventh dimensionless group is the ratio between the flap chord and the mean aerodynamic chord of the wing:

$$\pi_7 = \frac{c_f}{\sqrt{S}} = \frac{c_f}{c} = c_f/c \tag{5.8}$$

Therefore we obtain that the aeropropulsive force of our model can be described as:

$$C_F = C_F(M, Re, r_p, J, \alpha, \epsilon, SwfS, c_f/c, \delta_f) \tag{5.9}$$

The advantage of employing solely these dimensionless groups lies in using parameters that are independent of each other, thus covering all degrees of freedom of the model with the minimum number of parameters used.

## 5.2. Numerical campaign definition

In section 5.1, we identified the parameters required to describe the model in all its degrees of freedom.
However, to complete the entire numerical campaign, it would take an excessively long time to maintain all these parameter unfixed.
The High Lift Propellers are not operational in the cruise phase and it was therefore decided to set the Mach and Reynolds values to those typical of low speed and low altitude, thus considering an airspeed of 40 m/s and an altitude at sea level in standard ISA atmospheric conditions.
Furthermore, the dimensionless number $r_p$ remains constant during the design loop on Hyperion as the number and separation between the High Lift Propellers and the aspect ratio of the wing are predetermined and constant.
TITAN takes $H_i$ and $H_o$ as inputs, which denote the relative positions of flap start and flap end along the wingspan.

When TITAN operates without the meta model, it calculates the minimum required value of $c_f/c$ to achieve the specified minimum $\Delta C_L$ values during take-off and landing.
The additional ARGOS modules for sizing flaps in the presence of a flapped meta model, now utilize the $c_f/c$ number as an input rather than calculating it.
This input value have to match the one employed in constructing the meta model.
Note that once $H_i$ and $H_o$ are defined, the $S_f/S$ value is implicitly defined too; Therefore, since OpenVSP uses the first two parameters to define the flaps, they will be utilised to define the flap's characteristics rather than $S_f/S$.
Table 5.1 reports the fixed parameter values.

| | $M$ | $Re$ | $r_p$ |
|---|---|---|---|
| **Values** [-] | 0.114 | 3.99e+6 | 0.2976 |

Table 5.1: Fixed parameter in the numerical campaign.

The aim of the numerical study is to determine the value of $C_F$ leaving $\alpha$, $\epsilon$, $J$ and $\delta_f$ as the remaining independent variables that impose the metamodel space.
Table 5.2 presents the selected range for each independent variables used to construct the meta model.

| | **Initial range value** | **Final range value** |
|---|---|---|
| $\alpha$ [deg] | $-4$ | 16 |
| $\epsilon$ [deg] | $-12$ | 0 |
| $J$ [-] | 0.8 | 1.6 |
| $\delta_f$ [deg] | 0 | 30 |

Table 5.2: Range of parameters in the numerical campaign.

The values chosen by Moretti[10] and typical for the flight conditions in question were maintained for the $\epsilon$ and $J$ values.
Additionally, the chosen interval for the $\delta_f$ parameter was based on typical usage values for this type of flap [12]. In order to construct the polars, a specific range of the AoA is required; In this case, the range established by Moretti in his thesis has been maintained, and is divided into six equally spaced values, starting from -4° to 16°.
To further reduce computational costs, the isolated wing model was simulated.

As stated in Section 4.4, it has been decided to use the reduced Moretti method also for the configuration equipped with flaps; Each test point is obtained by simulating five different configurations. These configurations include exclusively $Prop_2$, $Prop_4$, and both two propellers couples to calculate the increases in $\Delta C_L$ and $\Delta C_D$ for each pair of propellers ranging from prop1 to prop4 and the $C_{Lu}$.
Two configurations were used to calculate the increases in $\Delta C_L$ and $\Delta C_D$ due to propellers outside the wing linearity zone, one using only $Prop_5$ and the other using only WTPs.
Figure 5.1 illustrates the configurations described above.


(a) $Prop_2$ model configuration.


(b) $Prop_4$ model configuration.


(c) $Prop_{24}$ model configuration.


(d) $Prop_5$ model configuration.


(e) $Prop_6$ model configuration.

Figure 5.1: Model configurations used for meta model construction.

Since the parameters describing the wing vary linearly with respect to the spanwise direction, calculating the total increase in lift and drag by summing the individual contributions of propeller pairs, offers another advantage: managing twisted wings using an untwisted wing model is possible.

It is indeed feasible to compute the local tilt and AoA behind each propeller of the twisted wing; Subsequently, utilizing simulations of the untwisted wing that match the already computed local parameters, the augmentations in $C_L$ and $C_D$ caused by that propeller can be computed; For further clarifications refer to [10].

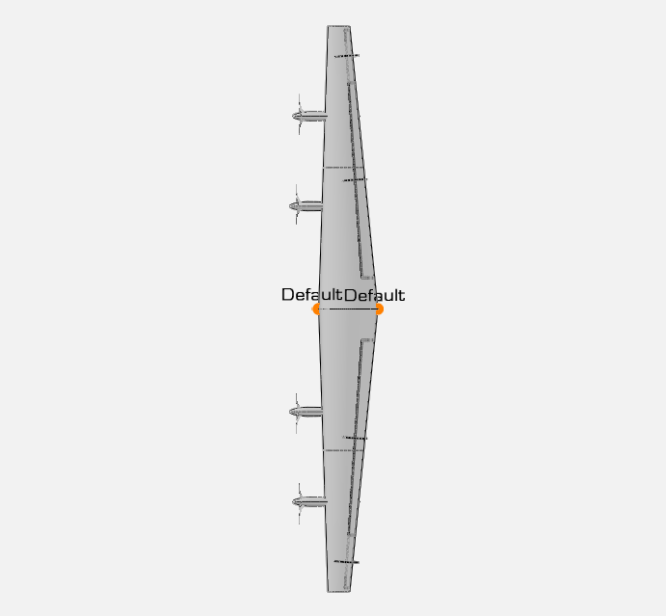


Figure 5.2: Representation of the model in configuration with propellers 2 and 4.

Figure 5.2 displays the model in a $Prop_{24}$ configuration with the propeller tilt at 0°; Table 5.3 gives all the geometric data of the wing, noting that, unlike the UNIFIER19 configuration, the C7A-HARW is not twisted.

| | Value |
|---|---|
| $b$ | 20.11 m |
| $\bar{c}$ | 1.54 m |
| $S$ | $28,90$ m$^2$ |
| $AR$ | 14 |
| $\Lambda$ | 0° |
| $\lambda$ | 0.37 |
| $\Gamma$ | $-2$° |
| $\alpha_t$ | 0° |
| $i_w$ | 0° |
| Airfoil | LS(1)-0413 MOD |
| $(t/c)_r$ | 0.195 |
| $(t/c)_t$ | 0.129 |

Table 5.3: Model's parameters in meta model numerical campaign.

## 5.3. Data elaboration

After correcting the corrupted data manually [10], the data is processed before building the meta model maps.
Specifically, the $C_L - \alpha$ curves are linearized through interpolation using a first-degree polynomial, while the polars are interpolated through a second-degree polynomial; The $C_T$ coefficient is interpolated through generic sinusoidal functions. Subsequently, the reduced Moretti method is applied.
Moretti's thesis demonstrates how the $C_L - \alpha$ curves in the unblown cases, obtained from simulations of the different values of the pitch and $J$ angles, are all almost identical;
He therefore calculated the average polars for the unblown cases and then corrected the calculated $\Delta C_L$ and $\Delta C_D$ values based on the old polars.
As flap deflection can affect the $C_L - \alpha$ and polar curves, the aforementioned process was repeated for each flap deflection value.
Multidimensional maps are created for $\Delta C_L$, $\Delta C_L$ and $C_T$ as they contribute to the generation of lift and drag.
Linear interpolation is used to determine these values for each combination of $\alpha$, $\epsilon$, $J$ and $\delta_f$ values within their range chosen in the numerical campaign.

The multidimensional maps describe the contribution of each propeller pair, enabling representation of twisted wings since local geometric angles can be calculated, and the equivalent condition for a pair of propellers in the twisted wing can be determined.

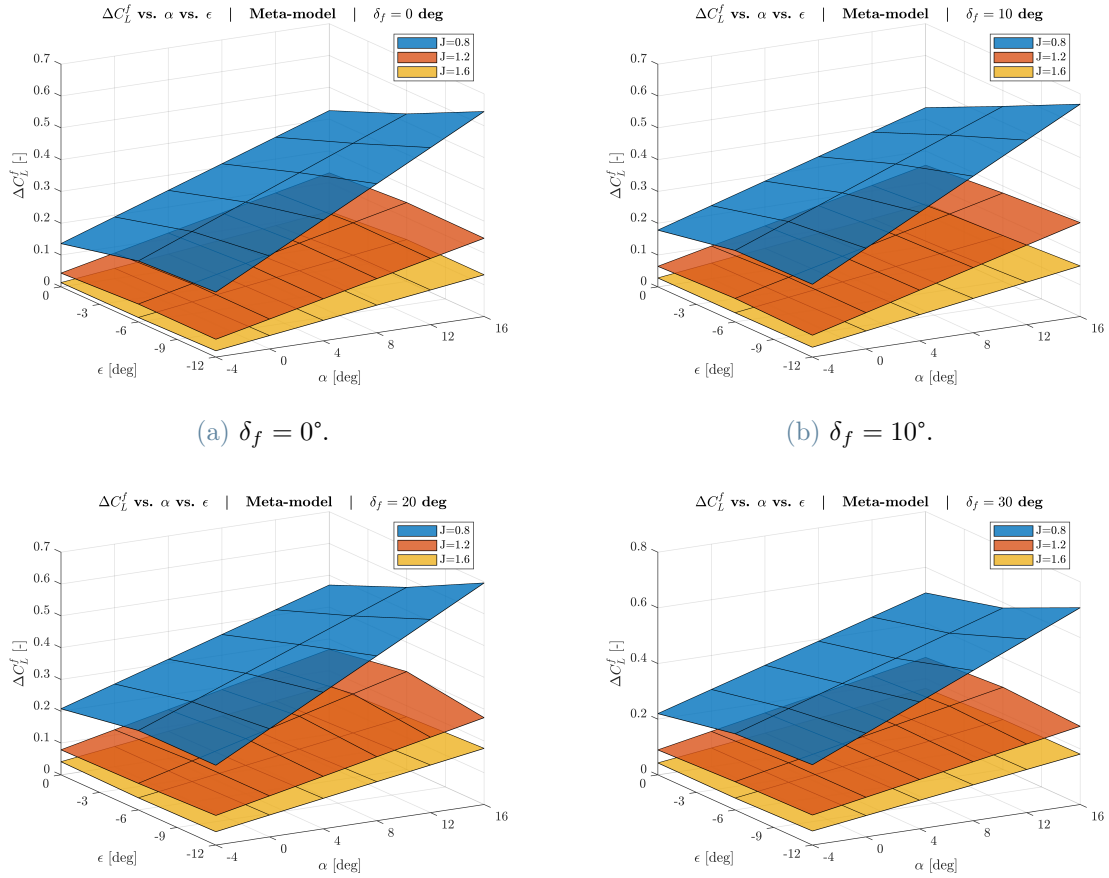


(a) $\delta_f = 0°$.

(b) $\delta_f = 10°$.

(c) $\delta_f = 20°$.

(d) $\delta_f = 30°$.

Figure 5.3: Increment of blown $C_L$ for the different flap settings.

Figure 5.3 shows for each $\delta_f$ setting, the total lift increment due DEP system, sum of the contributions of each propeller for all the $\alpha$ and $\epsilon$ combinations; The values of $J$ are instead fixed and are therefore displayed in the graph through different layers.

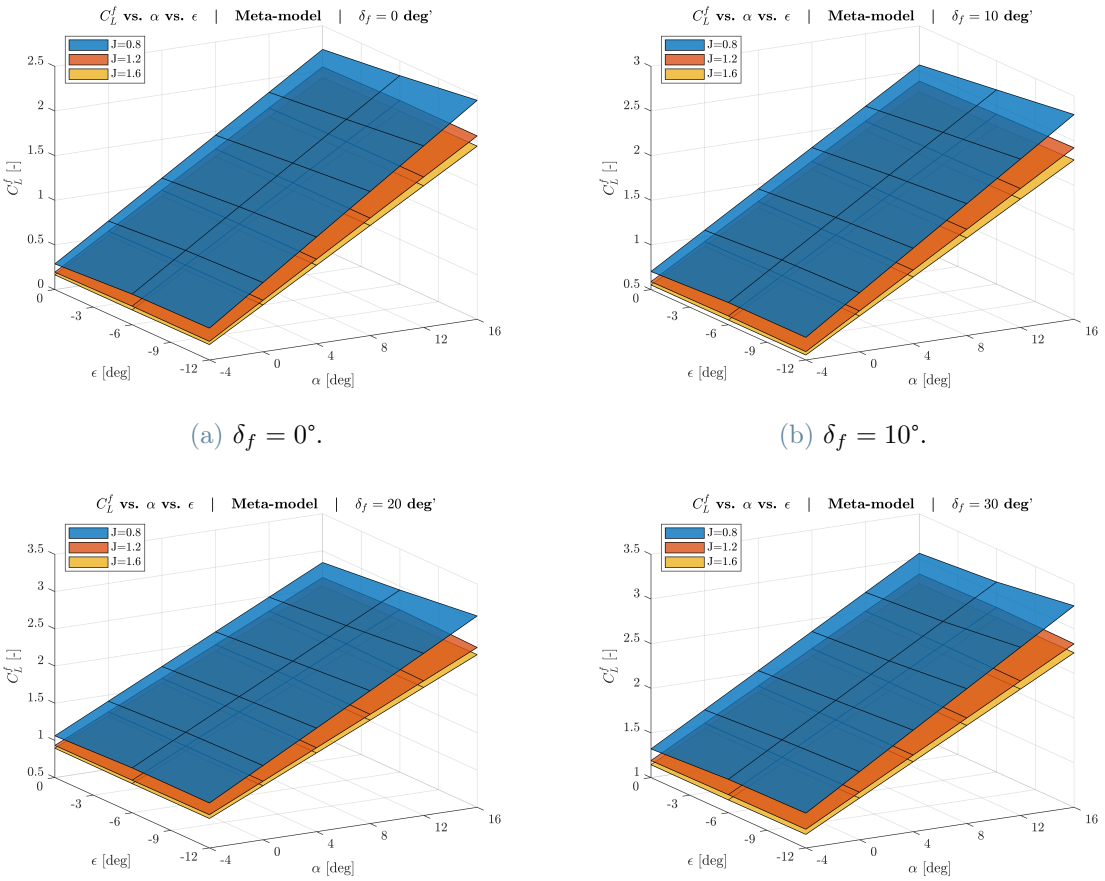


(a) $\delta_f = 0°$.

(b) $\delta_f = 10°$.

(c) $\delta_f = 20°$.

(d) $\delta_f = 30°$.

Figure 5.4: Lift coefficient in blown condition for the different flap settings.

Figure 5.4 presents for each $\delta_f$ setting, the lift coefficient value in blown condition for all combinations of $\epsilon$ and $\alpha$; Each layer displays the $J$ parameter.
By decreasing $J$ , there is an increase in $C_L$.
The difference between $J$ equal to 1.2 and 0.8 is significantly greater than the difference between $J$ equal to 1.6 and 1.2; indicating, since that the $C_{Lu}$ don't vary with $\epsilon$ and $J$, that $\Delta C_L$ is more sensitive to $J$ when it is lower, as visible in Figure 5.3.

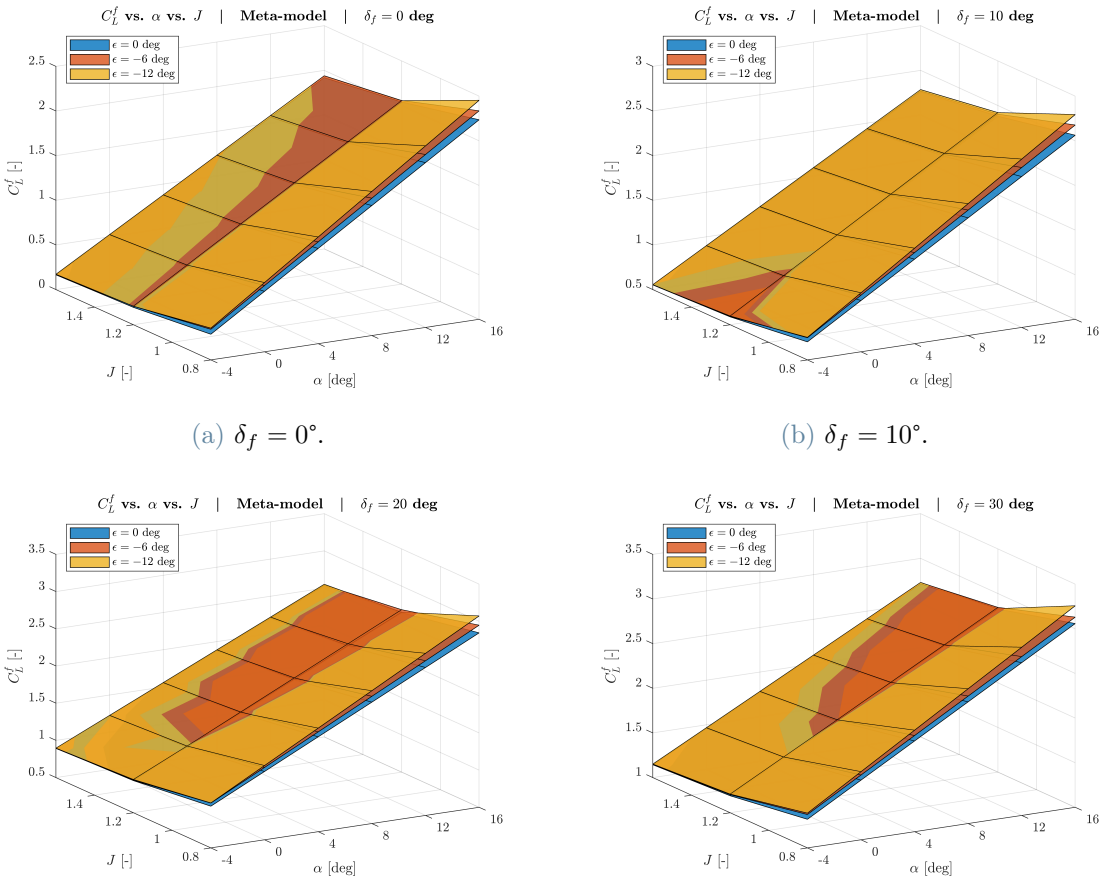


(a) $\delta_f = 0°$.

(b) $\delta_f = 10°$.

(c) $\delta_f = 20°$.

(d) $\delta_f = 30°$.

Figure 5.5: Lift coefficient in blown condition for the different flap settings.

Figure 5.5 shows the lift coefficient in the blown case as $J$ and $\alpha$ change.
The layers connected to each $\epsilon$ angle value are much closer than those presented in Figure 5.4, which are linked to each $J$ value. This implies a reduced sensitivity of $C_L$ to the tilt angle compared to $J$, especially for advance ratio between 1.2 and 1.6 between which the layers almost overlap.
This implies that controlling lift coefficient in the blown case using tilt angle is inadequate, particularly for advance ratio between 1.2 and 1.6.

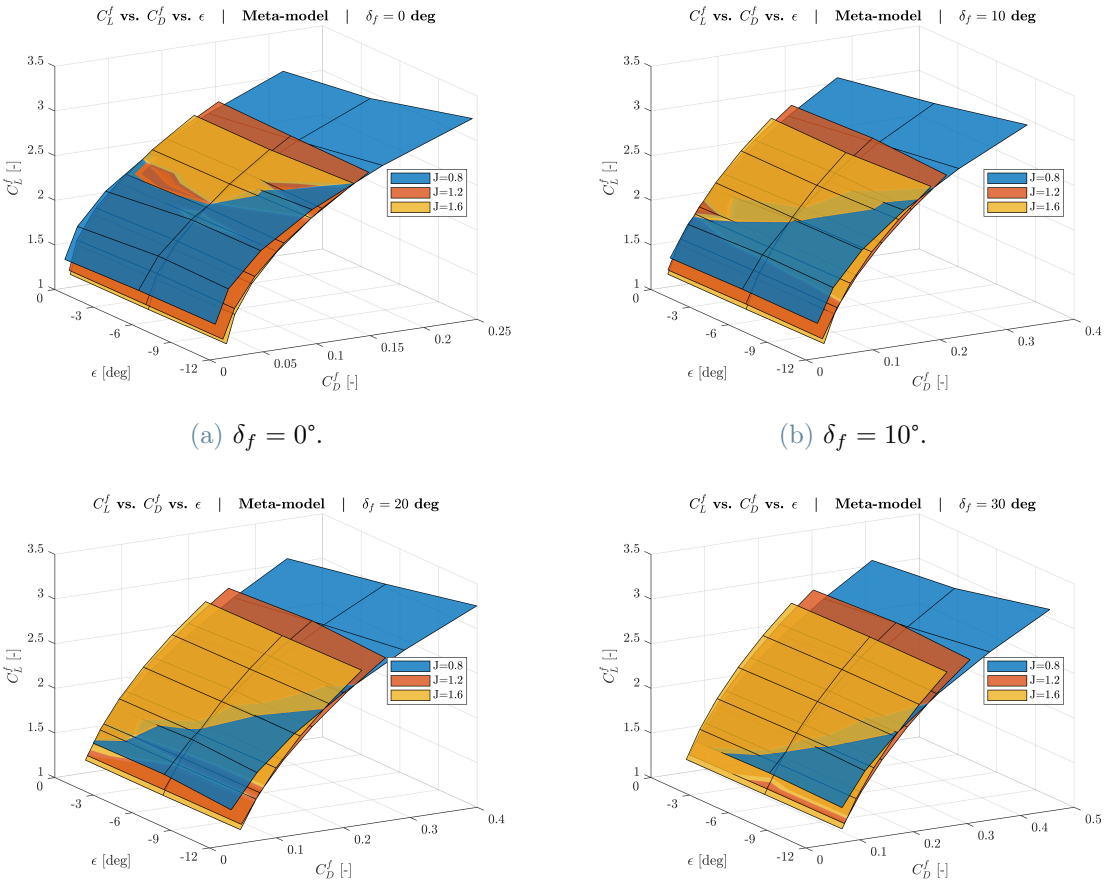


(a) $\delta_f = 0°$.

(b) $\delta_f = 10°$.

(c) $\delta_f = 20°$.

(d) $\delta_f = 30°$.

Figure 5.6: Multidimensional polar plot in blown condition and for the different flap settings.

Figure 5.6 displays the $C_L - C_D$ curves and consequently the polars as the tilt angle varies for each flap deflection; the different layers in the graphs represent the different values of $J$ instead.
These graphs provide various indications:

- There was a general increase in $C_D$ at both low and high AoA, indicating an increase in $C_{D0}$ and induced drag with flap deflection.
- For high AoA, high advance ratios are more efficient, as a wing subjected to a greater air flow will suffer from greater resistance; However, as shown in Figure 5.3 a low advance ratio is necessary to obtain a greater increase in lift, the main objective of the High Lift Devices.
- For $\delta_f$ of 0° and 10°, an advance ratio of 0.8 is advantageous for low CL values.

- For $\delta_f$ of 20° and 30°, along with low AoA, the study shows that high advance ratios are beneficial for tilt angles near 0°, while low advance ratios are favourable for tilt angles approaching -12°.

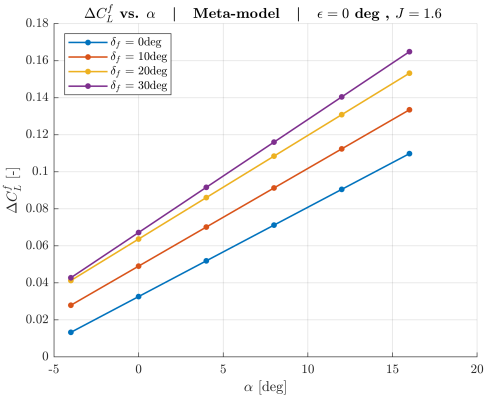


(a) $\Delta C_L$ for $\epsilon = 0°$ and $J = 1.6$.

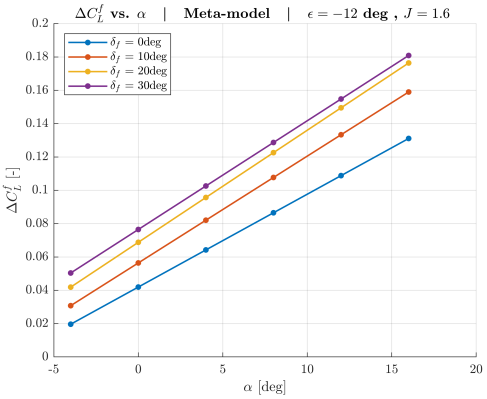


(b) $\Delta C_L$ for $\epsilon = 0°$ and $J = 1.6$.

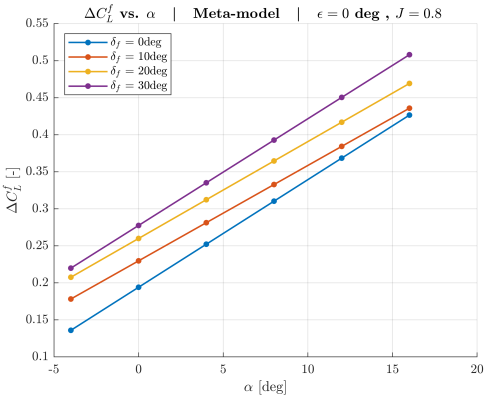


(c) $\Delta C_L$ for $\epsilon = 0°$ and $J = 1.6$.

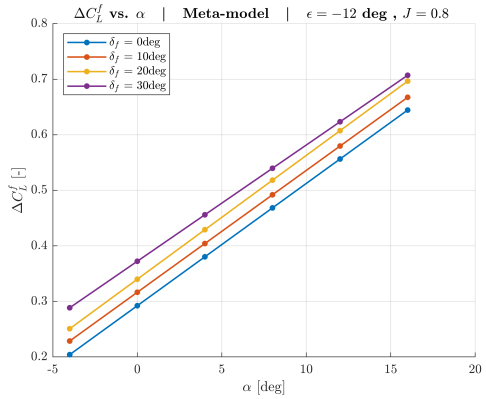


(d) $\Delta C_L$ for $\epsilon = 0°$ and $J = 1.6$.

Figure 5.7: Total increment of lift coefficient for different conditions.

Figure 5.7 displays the $\Delta C_L - \alpha$ curves. The tilt varies from 0° to -12° by moving from plots 5.7a to 5.7b and from 5.7c to 5.7d;
Likewise, the advance ratio decreases from 1.6 to 0.8 when transitioning from plots a to c and b to d, correspondingly.
Consistent with previous plots, there is evidence to suggest that the $\Delta C_L$ is more responsive to changes in the advance ratio than the tilt angle.
For J values of 1.6, a tendency of increasing slope is observed, whereas for the curves obtained with J = 0.8, a tendency of decreasing slope with flap deflection is noted.
In order to understand the causes of this behaviour, the contributions to the $\Delta C_L$ of each of the propellers are shown in Figure 5.8.

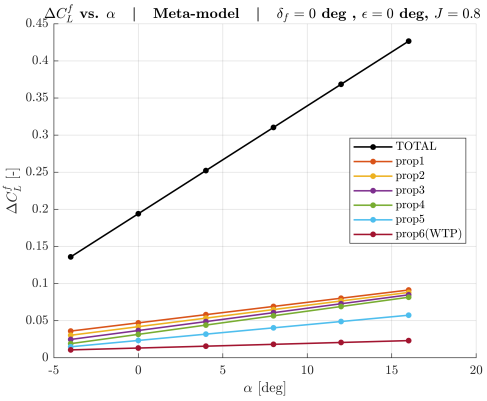


(a) $\delta_f = 0°$.

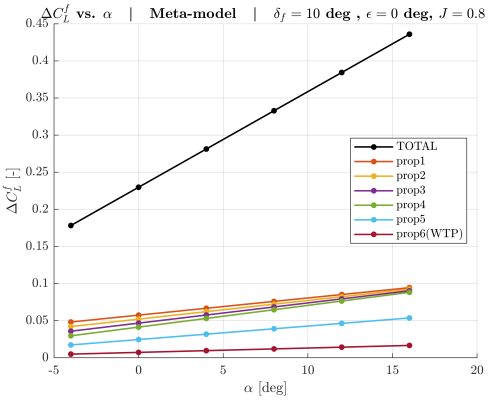


(b) $\delta_f = 10°$.

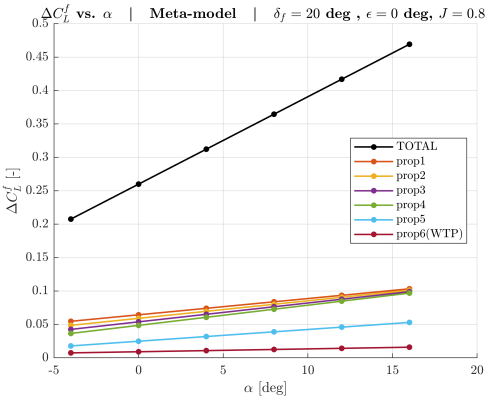


(c) $\delta_f = 20°$.

Figure 5.8: Contribution in lift increment of each propeller for $\epsilon = 0°$, $J = 0.8$ and different flap settings.

Firstly, we observe that the effects of $Prop_5$ and WTPs on $\Delta C_L$ remain steady when the flaps deflect. This is expected since the flows from these thrusters do not come into contact with the flaps, resulting in a constant wing geometry seen by these propellers when flap deflect.

It should be noted that in the case of undeflected flaps, the proportionality in the slope of $\Delta C_L$ contributions between $Prop_5$ and propellers 1 to 4 is lost, although there were no modifications to the parameters compared to the model without flaps.

Section 4.4 examines the $C_L$ obtained with the reduced method between $Prop_1$ and $Prop_4$ when compared to the reduced method between $Prop_1$ and $Prop_5$ at alpha $= 4°$; It is revealed that the second approach is more precise, but there are no issues with using the first method at least at this angle of attack.

For enhanced accuracy in calculating incremental coefficients in clean configurations, it is advisable to utilize the meta model with no flaps and obtained with the reduced method

between $Prop_1$ and $Prop_5$.
For configurations with flaps deflected, this behaviour is expected due to the higher camber in the flapped area of the wing.
Figure 5.9 illustrates how the previously described loss of proportionality at a tilt of 0° is considerably diminished when the tilt angle is -12°.

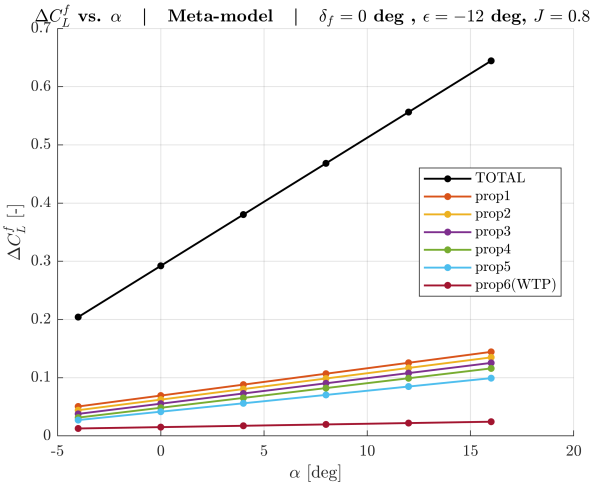


Figure 5.9: Contribution in lift increment of each propeller for $\epsilon = -12°$, $J = 0.8$ and $\delta_f = 0°$.

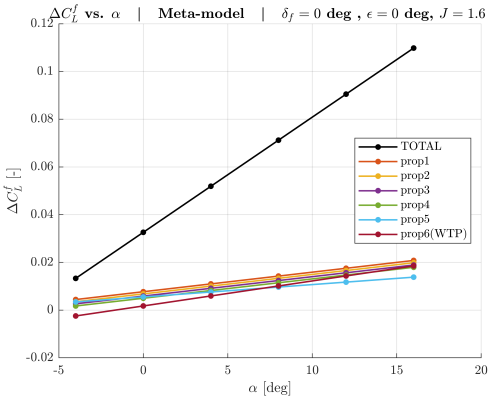


(a) $\delta_f = 0°$.

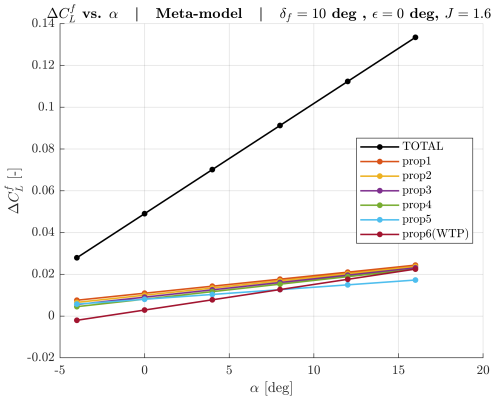


(b) $\delta_f = 10°$.

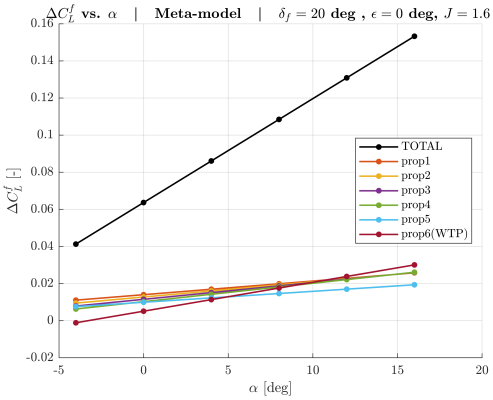


(c) $\delta_f = 20°$.

Figure 5.10: Contribution in lift increment of each propeller for $\epsilon = 0°$, $J = 1.6$ and different flap settings.

Figure 5.10 shows the contribution of each propeller to the increase of the lift coefficient in different flap configurations when the tilt angle is 0° and the $J$ is 1.6. This $J$ setting is associated with increases in lift coefficients that are reduced compared to those seen previously for the $J = 0.8$ cases, highlighting other characteristics:

- For $J = 1.6$, the increases in $\Delta C_{L5}$ and $\Delta C_{L6}$ due to the deflection of the flaps are comparable to those of the other propellers.
- WTPs are associated with a greater slope of $\Delta C_L$ compared to Prop5 due to the effect of WTPs on the contrast of the induced vortices, therefore the resistance component of the tip vortices will contribute to the generation of lift rather than induced drag.
- The contributions related to the other propellers do not differ from the considera-

tions made previously for the cases with $J = 0.8$.

Figure 5.11 shows the trend of $\Delta C_D$ as made in Figure 5.7 for the increase of lift;
In this case as well, there is a greater sensitivity to the $J$ parameter than to the tilt.
As for the $\Delta C_L$ scenario, the $\Delta C_D$ also demonstrates a dominance of the effects arising from $Prop_1$ to $Prop_4$ at $J = 0.8$.
Instead, at $J = 1.6$, all propellers have effects of similar magnitude.

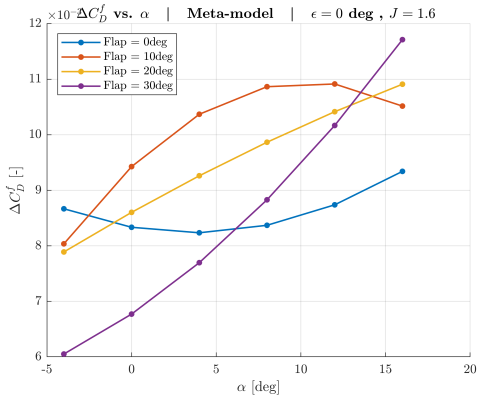


(a) $\delta_f = 0°$.

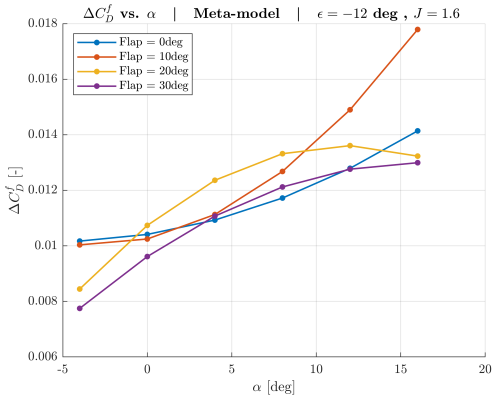


(b) $\delta_f = 10°$.

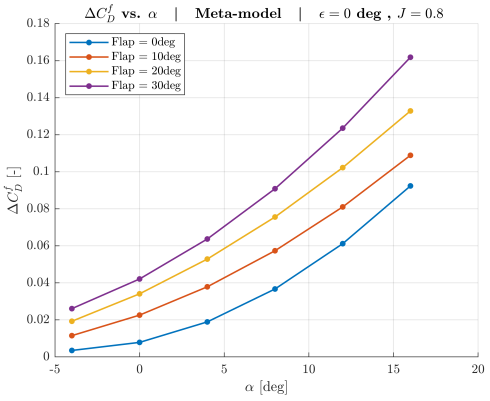


(c) $\delta_f = 20°$.

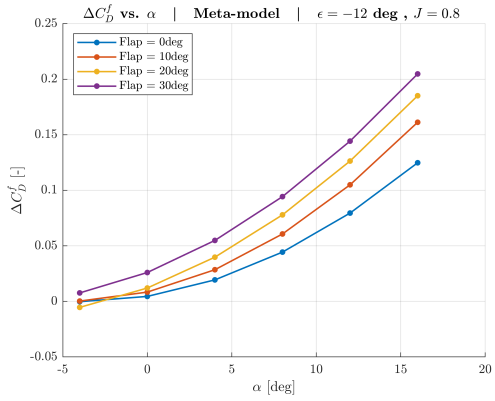


(d) $\delta_f = 20°$.

Figure 5.11: Contribution in drag increment of each propeller for $\epsilon = 0°$, $J = 1.6$ and different flap settings.

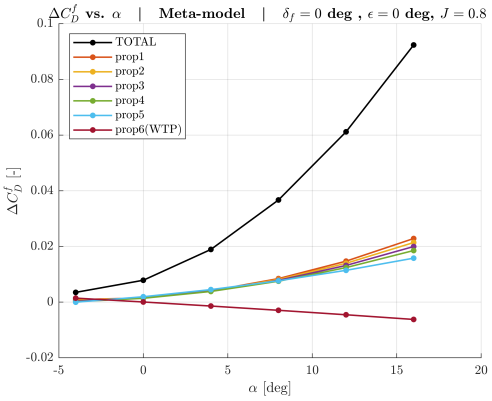


(a) $\delta_f = 0°$.

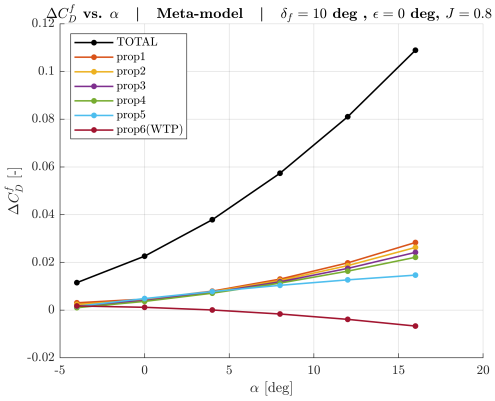


(b) $\delta_f = 10°$.

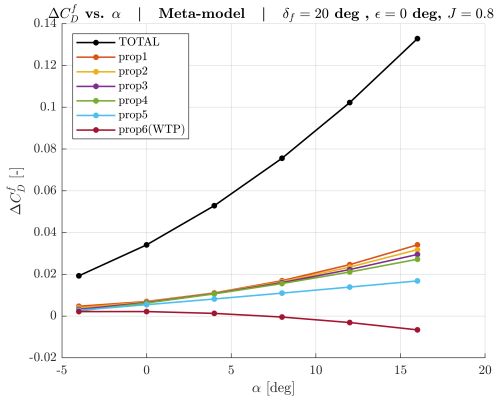


(c) $\delta_f = 20°$.

Figure 5.12: Contribution in drag increment of each propeller for $\epsilon = 0°$, $J = 0.8$ and different flap settings.

Figure 5.12 shows the contributions of each propeller to the change in drag coefficient for $J = 0.8$; $Prop_5$ and $Prop_6$ display less variation compared to $Prop_1$ to $Prop4$, which corresponds to the trends observed in the change in lift coefficient.

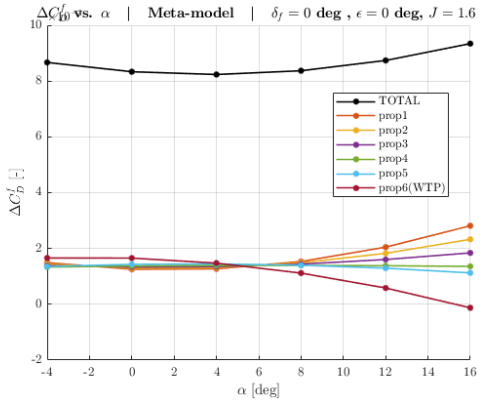


(a) $\delta_f = 0°$.

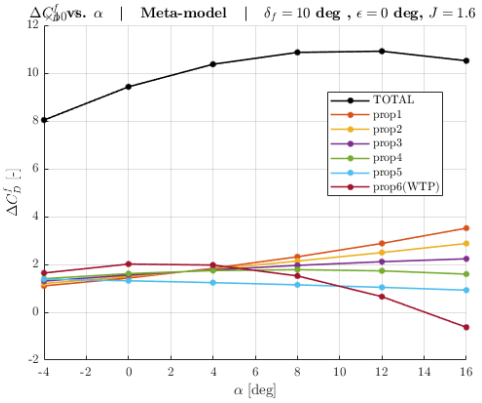


(b) $\delta_f = 10°$.

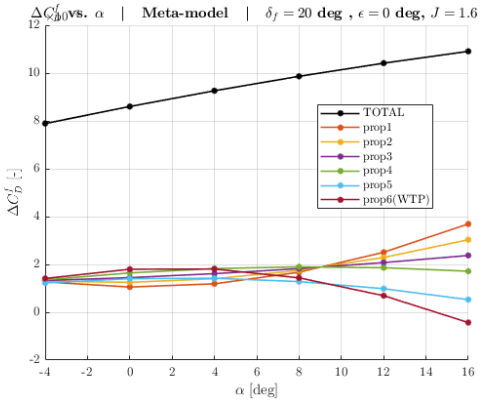


(c) $\delta_f = 20°$.

Figure 5.13: Contribution in drag increment of each propeller for $\epsilon = 0°$, $J = 1.6$ and different flap settings.

Figure 5.13 shows the effect of each propeller on the increasing in resistance coefficient for $J = 1.6$; As for $\Delta C_L$ all propellers have effects of similar magnitude.
In addition, these graphs highlight the greater $C_D$ reduction effect of WTPs with flap deflection.

# 6 | TITAN

This chapter outlines the structure of the Titan code, which has been developed by the Politecnico di Milano and enables the sizing of aircraft of categories CS23 and CS25.
The code is divided into blocks and the operational logic of TITAN without the presence of the meta-model will be illustrated, then the corresponding blocks added to integrate the meta-model into the sizing routine will be described.

## 6.1. TITAN sizing routine

The TITAN macro activity consists of combining two different tools in an iterative cycle until they produce the same solution [5]:

- The first tool is called Hyperion (HYbrid PERformance Simulation) and is a code capable of determining the design weights, based on a sizing mission, dimensioning the power-train components and wing general sizing i.e. surface area and span [5]; It's input consists in specification of the mission, regulation and the technological specifications of the power-train.
- The second tool, known as ARGOS (AiRcraft GeOmetric Sizing), is a design methodology that is able to provide a geometrical design of the entire aircraft, estimate its weight and predict its aerodynamic performance.

TITAN initiates by providing HYPERION with input based on the sizing mission; Afterwards, ARGOS takes some HYPERION output and other ARGOS-specific inputs based on the aircraft configuration.
HYPERION uses the non-propulsive airframe mass and aerodynamic data (parasite drag and Oswald factor) from ARGOS output as input [5].
This process is repeated until the solutions found by the two tools converge.
Figure 6.1 is an illustration of the TITAN procedure aforementioned.

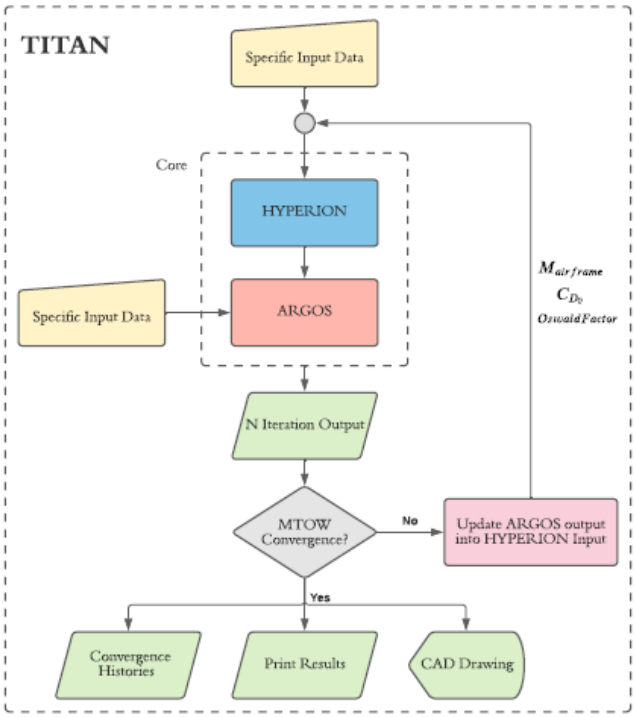


Figure 6.1: TITAN architecture [5].

## 6.2. Sizing procedure without meta model

It is reported hereafter the flaps related sizing procedure.
The HYPERION system includes among the inputs the maximum $C_L$ obtainable for each flap configurations.
To determine the increases in $C_L$ and $C_D$ due to the DEP system, HYPERION uses the Patterson's method [11] and [10].
As the meta-model is absent, Argos is unable to determine the impact of the DEP system on the rise of $C_L$ and $C_D$; Therefore, it assumes that the value obtained by HYPERION with Patterson's method is accurate.

The ARGOS modules correlated with meta-model integration are [10]:

- The **LLT module** sizes the wing selecting the optimal twist and taper to minimize the induced drag for cruise.
- The **HLD module** sizes the flaps and compute their deflection to ensure the requested increment of lift; Therefore, the attainment of the necessary $\Delta C_L$ will be

computed without taking into account the contribution provided by the DEP system.

- The **Performance module** estimates a parabolic polar, later fed to Hyperion for the next iteration.

To incorporate the meta-model into TITAN, Moretti [10] integrated two extra modules into ARGOS which are only activated by TITAN if the meta-model is available; thus the integrity of TITAN is maintained and it can work with the old routine if the meta-model is not available; For further information regarding this TITAN configuration refer to [10].

## 6.3. Architecture in presence of meta model equipped with flaps

New modules have been added into ARGOS, in order to integrate the meta-model equipped with flaps.
These modules are only activated when the meta-model provided with flaps is available, to ensure that the integrity of TITAN remains unaltered by avoiding changes to existing blocks.
If both the meta-model equipped with flaps and the one without flaps are present, the routine that utilize the first will be chosen.

The ARGOS blocks concerning the integration of the meta-model equipped with flaps into TITAN are:

- The **OverallHLD module** receives the geometric parameters of the flaps, it calculates the necessary flap deflection, and computes the required operational settings for the propeller during the relevant flight phases.
- The **PerfOverallHLD module** compute, for each flap configuration, the polar with the DEP system activated, obtaining the requested values computed in *OverallHLD.m*.
- The **CorrectionFlapTO module** and the **CorrectionFlapL module** are activated in case that occurs $P_{\%}^{DEP} > 100\%$ or $\sigma_{DEP} > 100\%$, as in these instances, the power and thrust generated by the HLP exceed the requirements for the trimmed flight condition.
  This has been corrected by these new modules, by increasing the flap deflection and reducing the lift increment provided by DEP system.
  $P_{\%}^{DEP}$ and $\sigma_{DEP}$ parameters are explained at the end of this section.

In order to implement these blocks in TITAN, the following procedure is carried out.
The Matlab file *simsReader.m* implemented by Moretti [10] and used to acquire data from VLM simulations, it is updated with the new $\delta_f$ parameter.
The *preProcessor.m* Matlab file implemented by Moretti [10] has been modified to include the flap deflection parameter, in particular the unblown polar averaging is performed separately for each flap deflection.
It has also been modified to use the reduced approach from Prop1 to Prop4 as described in section 4. The Matlab file *preProcessor.m* is the one which creates the multidimensional maps.
Once the meta-model equipped with flaps has been created; the description of the blocks involved in its integration in ARGOS is proposed.
*OverallHLD.m* take as input the geometric inputs of the flap, note that now also the $c_f/c$ is treated as input and is no longer calculated, as the operator will have to set the same value that will be used for the meta-model.
Starting from the maximum lift coefficient specified for HYPERION, the $\Delta C_L$ is calculated for each flap configuration.
The Patterson's function is used to determine for each flap configuration the $\delta_f$ for which the lift increase in the unblown condition due flap and the lift increase provided by the DEP system on the flap deflected wing give the desired lift increase.
By using meta-model maps, it is determined the required advance ratio, which provides the lift increment required from the DEP system;
For the treatment of local AoA and local tilt angle, in order to replicate the twisted wing local angles, consult [10].
Finally, the operational HLP settings and the total thrust coefficient produced by the DEP system are derived.
OverallHLD is part of the wing geometry determination modules
Passing to the performance modules, *PerfOverallHLD.m* is the one responsible for correcting the polar for each flap configuration.
For all ranges of local AoA available with the alpha range offered by the meta-model, the $C_{Lu}$ and the resulting $C_{Du}$ are calculated with the actual flap deflection.
By using the $C_{Lu}$ found, it is computed in according to Patterson the target $\Delta C_L$ provided by the DEP system; thus trough the meta-model maps at the actual local alpha, it is computed the necessary $J$ to reach that coefficient lift increase.
Knowing the local alpha and $J$, the increase in $C_D$ caused by the DEP system are found through the use of meta-model maps.
The parabolic approximation is applied to the established polars, thus obtaining the $C_{D0}$ and the Oswald factor ($e$) for the relative flap condition.

The $C_{D0}$ derived from the clean polar configuration is used to update the $C_{D0}$ with the resistance nacelles contribution;
The polars obtained from flapped configurations with the DEP system operating are used to update the flap contribution to $C_{D0}$ and the Oswald factor ($e$), for both take-off and landing configurations.
In particular, the flap contribution to $C_{D0}$ is calculated by subtracting the $C_{D0}$ obtained from the blown polar in flapped configuration with the $C_{D0}$ from the blown polar in clean configuration, which has already been updated with the nacelle contributions.
Finally, the DEP power ratio and DEP throttle parameters are estimated for each of the five significant flight conditions [10] considered in the lift augmentation module.
The first is the ratio between the available DEP power and the required power in the specified condition [10]:

$$P_{\%}^{DEP} = \frac{P_a^{DEP}}{P_r} = \frac{T^{DEP}V}{DV} = \frac{2d^2C_T^{DEP}}{SJ^2C_D}, \tag{6.1}$$

The second is the ratio between the actual DEP shaft power in the specified flight condition and the Maximum Continuous Power of the DEP system [10]:

$$\sigma_{DEP} = \frac{P_a^{DEP}}{P_r} = \frac{T^{DEP}V}{\eta_p^{DEP}P_b^{DEP}} = \frac{\rho V^3 d^2 C_T^{DEP}}{J^2\eta_p^{DEP}P_b^{DEP}}, \tag{6.2}$$

## 6.4. Results comparison

This section compares the three TITAN results: with no meta-model, with the meta-model without flap and with the meta-model equipped with flap.
All three results are obtained by entering the same inputs as those settled by Moretti [10] to replicate the aircraft UNIFIER19 in configuration C7A-HARW, for more datail refer to [10].
Table 6.1 reports the input concerning the flap characteristic for the three TITAN configurations; The values are the same for all TITAN configurations, except for the $c_f/c$, since it is an input for the meta-model with flap case and an output for the other cases, in which the minimum value necessary to obtain the required lift is taken. Coincidentally, the $c_f/c$ values are the same in the three versions, In fact this is a very common value for this type of flap. The $SwfS$ isn't directly settled in the input file, but is fully defined when $H_I$ and $H_O$ are settled.

| | No meta-model | Meta-model without flap | Meta-model with flap |
|---|---|---|---|
| $H_I$ [-] | 0.11 | 0.11 | 0.11 |
| $H_O$ [-] | 0.8 | 0.8 | 0.8 |
| $SwfS$ [-] | 0.72 | 0.72 | 0.72 |
| $c_f/c$ [-] | 0.25 (output) | 0.25 | 0.25 |

Table 6.1: Input related to flap for each TITAN configuration.

The sizing mission is the one settled by Moretti [10] and plans six hops of 350 km each, at 4000 ft and 141.4 kn; a 100 km diversion to an alternate airport and a loiter of 45 minutes follow the first hop [10].
This mission design is intended to ensure the capability to fly to many small airports without the need to refuel and recharge batteries, due to the lack of facilities and infrastructure at small airports [6].

| | Values |
|---|---|
| **Single hop range** | 350 km |
| **Number of hops** | 6 |
| **Cruise altitude** | 4000 ft |
| **Cruise speed** | 141.4 kn |
| **Diversion range** | 100 km |
| **Loitering time** | 45 min |

Table 6.2: Sizing mission settings [10].

For this new TITAN configuration, a different strategy is used to calculate the required flap deflection; now the required $\Delta C_L$ is obtained thanks to the sum of the flap deflection contribution and the DEP system contribution at that flap deflection.
This results in a smaller $\delta_f$ required, as seen in Table 6.3 for both take-off and landing cases.

| | No meta-model | Meta-model without flap | Meta-model with flap |
|---|---|---|---|
| $\delta_{f,TO}$ [°] | 11 | 11 | 7 |
| $\delta_{f,LND}$ [°] | 35 | 35 | 17 |
| $c_f/c$ [-] | 0.25 (input) | 0.25 | 0.25 |

Table 6.3: Output related to the flaps for each TITAN configuration.

Table 6.4 shows the polar parameters obtained for all TITAN configurations, for the flight conditions clean and with flaps deflected for take-off and landing.
$C_{D0}$ is updated for clean flight condition to consider nacelles contribution; $C_{D0}$ is increased with respect to the one obtained with the meta-model not provided with a flaps, perhaps due to the reduced method used; As reported in Section 4.4, it is associated with less precision for this flight configuration.
In this thesis we have only used the meta-model equipped with flaps, to compare the results with those of other versions of TITAN in all flight conditions;
However, for future applications of TITAN, for the calculation of the $C_{D0}$ in clean configuration, we recommend the use of the meta-model without flaps or ad hoc simulations carried out with the DEP system not working.
The ARGOS routine does not consider updating the Oswald factor for this flight condition as the DEP system is not working.
Considering the DEP contribution in a more cambered wing due to flap deflection, in the take-off configuration a greater increase of $C_{D0}$ is observed with respect to that obtained with the meta-model without flaps.
Due to the augmented flap deflection and the reduced DEP system contribution in the landing configuration, to reduce $\sigma_{DEP}$ and $P_{\%}^{DEP}$ below 100%, there is a reduced blowing effect, thus reducing the $C_{D0}$ with respect to the take-off configuration.

| Flight condition | Polar parameter | No meta-model | Meta-model without flap | Meta-model with flap |
|---|---|---|---|---|
| clean | $minC_D$ | 0.0402 | 0.0489 | 0.0525 |
| | $e$ | 0.657 | 0.657 | 0.657 |
| Take-off | $minC_D$ | 0.0415 | 0.0503 | 0.0618 |
| | $e$ | 0.800 | 0.876 | 0.839 |
| Landing | $minC_D$ | 0.0734 | 0.0821 | 0.0604 |
| | $e$ | 0.750 | 0.826 | 0.685 |

Table 6.4: Polar parameter for each flight and TITAN configurations.

| Flight condition | HLP parameter | No meta-model | Meta-model without flap | Meta-model with flap |
|---|---|---|---|---|
| stall (clean) | $N$ [RPM] | – | 1285 | 1270 |
| | $\sigma$ [%] | – | 28 | 26 |
| | $P_{\%}^{DEP}$ [%] | – | 30 | 27 |
| stall (TO) | $N$ [RPM] | – | 1390 | 1377 |
| | $\sigma$ [%] | – | 51 | 51 |
| | $P_{\%}^{DEP}$ [%] | – | 60 | 54 |
| TO speed | $N$ [RPM] | – | 1299 | 1226 |
| | $\sigma$ [%] | – | 37 | 26 |
| | $P_{\%}^{DEP}$ [%] | – | 39 | 25 |
| stall (LND) | $N$ [RPM] | – | 1573 | 1582 |
| | $\sigma$ [%] | – | 86 | 89 |
| | $P_{\%}^{DEP}$ [%] | – | 95 | 85 |
| LND speed | $N$ [RPM] | – | 1315 | 1177 |
| | $\sigma$ [%] | – | 41 | 21 |
| | $P_{\%}^{DEP}$ [%] | – | 37 | 19 |

Table 6.5: HLP settings for each TITAN configuration.

Table 6.5 reports the HLP settings for the three TITAN version.
Since Titan doesn't calculate these values in case the meta-model isn't present, no data

is reported.
By considering the $\Delta C_L$ as the sum of the unblown effect and the contribution of the DEP system, leads to a significant decrease in $N$, $\sigma_{DEP}$ and $P_{\%}^{DEP}$ for the take-off and landing speed flight cases;
In the case of landing speed flight, the decrease in these values is slightly amplified by the reduction in the contribution of the DEP system to reduce $\sigma_{DEP}$ and $P_{\%}^{DEP}$ below 100%.
Table 6.6 compares the most relevant TITAN outputs, the final result in the case of the meta-model with flaps is a further increase in maximum take-off mass, fuel mass, the wing surface, and the shaft powers, while respect to the other TITAN versions.
A more detailed study of the obtained masses will follow.

| | **No meta-model** | **Meta-model without flap** | **Meta-model with flap** |
|---|---|---|---|
| $M_{TO}$ [kg] | 8071.6 | 8211.2 | 8281.6 |
| $S$ [m$^2$] | 28.29 | 28.74 | 28.99 |
| $P_b$ [kW] | 1304.9 | 1325.5 | 1337.0 |
| $P_b^{DEP}$ [kW] | 869.6 | 887.8 | 912.1 |
| $M_{LH_2}$ [kg] | 372.1 | 424.5 | 446.2 |

Table 6.6: Solutions of UNIFIER19-C7A-HARW for each TITAN configuration.

The first comparison concerns the $M_{TO}$, the total weight of the aircraft at take-off; this parameter is very important as it is closely correlated to the aerodynamic and structural characteristics of the aircraft.
It is also interesting to divide the masses into further categories, called breakdown masses, based on the components scope:

- **Crew + Payload** is a HYPERION input as it is one of the sizing mission requirements.
- **LH2 related** comprises all the components involved in the energy production from hydrogen; So including the fuel itself, the storage and conversion into electrical energy.
- **Battery**.
- **Structure + Systems** groups together all others components.

Table 6.6 shows all these mass values for the different TITAN configurations, while Table 6.8 shows the masses variation using as reference the TITAN results for the configu-

ration without the meta-model.
Structure + Systems masses are moderately sensitive to the new implementation applied in TITAN;
On the other hand, the LH2 related masses continue to suffer TITAN refinement with a relative variation increased from 13.9%, obtained with the meta-model without flap, to 20%; as observed in Table 6.8.
Crew + Payload mass doesn't vary by changing the TITAN configuration because this mass is a parameter of the sizing mission and therefore an input file.
Hence, the variations reported in Table 6.8 in relation to this mass are equal to zero.
The trend identified by Moretti [10] is also intensified for the battery mass, with a greater reduction of this mass using the meta-model equipped with flaps.
Adding up all the contributions of these masses, the $M_{TO}$ increase is of 2.4% respect to the result obtained without the meta-model, against the 1.7% found using the meta-model without flap.
All reasoning made by Moretti [10] mantain validity and are amplified when the meta-model provided with flaps is used:

- The increase in $C_{D0}$ is emphasised because the DEP system acts on a more cambered wing due to flap deflection, thus a greater amount of energy is required in the cruise phase; with a consequent increase in fuel mass and power generator mass required, as the latter must convert fuel into electrical energy at a higher rate.
- The increased power of the generator system reduces the amount of energy required from the battery to meet the peak power demanded during take-off.

| **Mass categories** | **No meta-model** | **Meta-model without flap** | **Meta-model with flap** |
|---|---|---|---|
| Structure + Systems [kg] | 4086.7 | 4136.1 | $4149,4$ |
| Crew + Payload [kg] | 2380.0 | 2380.0 | 2380.00 |
| LH2 related [kg] | 938.4 | 1069.3 | 1126.5 |
| Battery [kg] | 681.7 | 641.3 | 625.7 |
| TOTAL ($M_{TO}$) [kg] | 8086.8 | 8226.7 | 8281.6 |

Table 6.7: Mass values for each category.

| | | Structure + Systems | Crew + Payload | LH2 related | Battery | TOTAL ($M_{TO}$) |
|---|---|---|---|---|---|---|
| **Meta-model without flap variation tipology** | **Absolute** [kg] | 49.4 | 0 | 130.9 | -40.4 | 139.9 |
| | **Relative** [%] | 1.2 | 0 | 13.9 | -5.9 | 1.7 |
| **Meta-model with flap variation tipology** | **Absolute** [kg] | 62.7 | 0 | 188, 1 | -56 | 194, 8 |
| | **Relative** [%] | 1.5 | 0 | 20 | -8.2 | 2.4 |

Table 6.8: Mass variations for each category, TITAN's results from configuration without the meta-model used as reference.

# 7 | Conclusions

In conclusion, OpenVSP version 3.23 prove to be the better choice to replicate the already validated results found by Moretti [10].
The Sinnige's model equipped with flaps gave the results previously hypothesised, making it clear that the VLM method is idoneous tho evaluate the aerodynamics of a wing equipped with flaps.
The reduced method of Moretti proves to be applicable, even if with less precision in replicating, for the clean configuration, the data obtained from the simulation with all the propellers working; Therefore, this method of data acquisition and processing was chosen.
Finally, the results obtained by TITAN using the meta-model provided of the flaps had the amplified trend, respecting the results obtained without the meta-model, found by Moretti;
The refinement of the model leads to a further increase of the $C_{D0}$ in all flight conditions, respecting those found by Moretti [10], with a consequent increase of the masses, except for the battery one.
It is reasonable to consider that the effect of the DEP on a more cambered wing due to the deflection of the flaps leads to an increase in drag; but in the future, for the clean configuration phases, it is recommended to use data from the meta-model without flaps or use ad-hoc unblown simulations to compute the nacelle contribution.

# Bibliography

[1] Clean aviation webpage. URL https://clean-aviation.eu/.

[2] Nasa webpage. URL https://www.nasa.gov/image-detail/x-57_maxwell_water/.

[3] Nasa advanced air transport technology (aatt) webpage. URL https://www.nasa.gov/aeroresearch/programs/aavp/aatt/.

[4] ABBOT and DOENHOFF. Theory of wing sections. URL https://vspu.larc.nasa.gov/training-content/chapter-1-vspfundamentals/cross-section-details/naca-6-series-airfoil/.

[5] A. E. BRIZ, I. RAIMO, L. TRAINELLI, C. RIBOLDI, and A. ROLANDO. A framework for hybrid-electric aircraft preliminary sizing. 2019-2020. URL https://www.politesi.polimi.it/handle/10589/166438.

[6] M. DEL GRANO, L. TRAINELLI, and F. SALUCCI. Optimal approach to the preliminary sizing of hydrogen-driven transport aircraft. 2020-2021. URL https://www.politesi.polimi.it/handle/10589/183637.

[7] A. DETTMANN. Pytornado theory introduction webpage. URL https://pytornado.readthedocs.io/en/latest/theory/.

[8] R. MCDONALD, B. LITHERL, J. GRAVETT, J. GLOUDEMANS, M. MOORE, A. HAHN, B. FREDERICKS, and A. GARY. Wingtip-mounted propellers: Aerodynamic analysis of interaction effects and comparison with conventional layout. URL http://openvsp.org/.

[9] C. MONTSARRAT, B. DEVEAUX, J. BOUDET, J. MARTY, and E. LIPPINOIS. Vortex lattice method for the calculation of the tip leakage flow: Evaluation on a single blade. Sep 2020. URL https://hal.science/hal-03064945/document.

[10] A. R. MORETTI, L. TRAINELLI, and C. D. RIBOLDI. Mid-fidelity modeling of the aero-propulsive interaction for the initial design of distributed propulsion aircraft. 2021-2022. URL https://www.politesi.polimi.it/handle/10589/191677.

[11] M. D. PATTERSON. Conceptual design of high-lift propeller systems for small electric aircraft". 2016.

[12] D. P. RAYMER. Aircraft design: A conceptual approach.

[13] T. SINNIGE, N. VAN ARNHEM, T. C. A. STOKKERMANS, E. GEORG, and L. L. M. VELDHUIS. Wingtip-mounted propellers: Aerodynamic analysis of interaction effects and comparison with conventional layout. pages 295–312, 2019.

[14] A. A. SONIN. A generalization of the -theorem and dimensional analysis. URL https://www.pnas.org/doi/10.1073/pnas.0402931101.

# List of Figures

# List of Tables

# List of Symbols and Acronyms

| Symbol | Description |
|---|---|
| $\alpha$ | Angle of Attack |
| $\alpha_t$ | Wing twist |
| $\beta_{3/4}$ | Blade pitch at 75%R |
| $\Gamma$ | Wing dihedral |
| $\delta_f$ | Flap deflection |
| $\Delta C_D$ | Drag coefficient increment |
| $\Delta C_L$ | Lift coefficient increment |
| $\epsilon$ | Propeller tilt with respect to wing reference frame |
| $\eta_p^{DEP}$ | DEP propulsive efficiency |
| $H_I$ | Flap inner point respect to the wing spanwise |
| $H_O$ | Flap outer point respect to the wing spanwise |
| $\lambda$ | Wing taper ratio |
| $\Lambda$ | Wing sweep |
| $\Lambda_{H.L.}$ | Sweep angle of the flap hinge line |
| $\mu$ | Air dynamic viscosity |
| $\rho$ | Air density |
| $\sigma_{DEP}$ | DEP motors throttle parameter |
| $a$ | Speed of sound |
| $AR$ | Aspect ratio |
| $b$ | Wing spanwise |
| $c$ | Generic wing chord |
| $\overline{c}$ | Mean aerodynamic chord |
| $c_f/c$ | Flap chord and wing chord ratio |
| $C_D$ | Drag coefficient |
| $C_{D0}$ | Parassite drag coefficient |
| $C_{L\alpha}$ | Lift curve slope |
| $C_{L,min_{CD}}$ | Lift coefficient associated with the effective $minC_D$ |

| | |
|---|---|
| $C_{Lu}$ | Unblown wing lift coefficient |
| $C_T$ | Thrust coefficient ($\frac{T}{\rho N^2 d^4}$) |
| $d$ | Propeller diameter |
| $D$ | Drag |
| $e$ | Oswald factor |
| $i_w$ | Wing root incident |
| $J$ | Advance ratio ($\frac{V}{Nd}$) |
| $K$ | Drag polar concavity |
| $minC_D$ | Minimum drag coefficient |
| $L$ | Lift |
| $M$ | Mach number |
| $M_{LH_2}$ | Mass of liquid hydrogen |
| $M_{TO}$ | Maximum Takeoff Mass |
| $N$ | Propeller speed |
| $P_b$ | Shaft power |
| $P_r$ | Required power |
| $R$ | Propeller radius |
| $Re$ | Reynolds number |
| $r_h$ | Hub radius |
| $r_p$ | Geometrical parameter ($d/\sqrt{S}$) |
| $S$ | Wing surface |
| $S_{wf}$ | Flapped wing surface |
| $SwfS$ | Flapped wing surface and wing surface ratio |
| $t/c$ | Airfoil thickness ratio |
| $T$ | Thrust |
| $P_{\%}^{DEP}$ | Ratio of DEP available power over total required power |
| $V$ | Airspeed |
| $Y$ | Generic coordinate along y-body axis |
| $(.)_{,\delta_f}$ | Prime derivative with respect to the flap deflection |
| $(.)^{DEP}$ | Referred to DEP system |
| $(.)_i$ | Referred to the i-th propeller |
| $(.)_r$ | Referred to wing root |
| $(.)_t$ | Referred to wing tip |
| $(.)^w$ | Wing contributions |
| $(.)^f$ | Fixed group contributions |

| Acronyms | Description |
|---|---|
| $AoA$ | Angle of Attack |
| $AR$ | Aspect Ratio |
| $CFD$ | Computational Fluid Dynamics |
| $CS$ | Certification Specifications |
| $DEP$ | Distributed Electric Propulsion |
| $DP$ | Distributed Propulsion |
| $Exp$ | Experimental |
| $HARW$ | High Aspect Ratio Wing |
| $HLD$ | High Lift Device |
| $HLP$ | High Lift Propeller |
| $LND$ | Landing |
| $MAC$ | Mean Aerodynamic Chord |
| $MM$ | Meta-Model |
| $MWP$ | Mid-Wing Propeller |
| $RPM$ | Revolutions Per Minute |
| $TO$ | TakeOff |
| $VLM$ | Vortex Lattice Method |
| $VTP$ | Wingtip Propeller |